AIR FORCE OFFICE OF SCIENTIFIC RESEARCH

FINAL REPORT

for period January 15, 1993 to March 14, 1997

GRANT NO. F46920-93-1-0111

entitled

MBE GROWTH OF GaInAsSb

by

Shanthi N. Iyer

DEPARTMENT OF ELECTRICAL ENGINEERING
NORTH CAROLINA A & T STATE UNIVERSITY
GREENSBORO NC 27411

APPROVED FOR PUBLIC RELEASE;
DISTRIBUTION UNLIMITED

REPORT DOCUMENTATION PAGE

Form Approved
OMB No. 0704-0188

1. AGENCY USE ONLY (Leave blank)	2. REPORT DATE	3. REPORT TYPE AND DATES COVERED
	7/23/97	Final Report 1/15/93-3/14/97

4. TITLE AND SUBTITLE

MBE Growth of GaIn AsSb

5. FUNDING NUMBERS

F49620-93-1
-0111DEF

6. AUTHOR(S)

S. Iyer

7. PERFORMING ORGANIZATION NAME(S) AND ADDRESS(ES)

North Carolina A&T State University
Department of Electrical Engineering
Greensboro, North Carolina 27411

8. PERFORMING ORGANIZATION REPORT NUMBER

9. SPONSORING/MONITORING AGENCY NAME(S) AND ADDRESS(ES)

Major Michael Prairie
AFOSR/NE
110 Duncan Avenue Room B115
Boiling AFB, D.C. 20332-8080

10. SPONSORING/MONITORING AGENCY REPORT NUMBER

11. SUPPLEMENTARY NOTES

12a. DISTRIBUTION/AVAILABILITY STATEMENT

Approved for Public Release and Distribution
Unlimited.

12b. DISTRIBUTION CODE

13. ABSTRACT *(Maximum 200 words)*

Optimum growth conditions for high quality growth of GaAs, GaSb, InSb and GaInAsSb epilayers by Molecular Beam Epitaxy (MBE) on GaAs substrates and homo-epitaxial growth of InSb have been determined. A new procedure for expeditious removal of oxide desorption from InSb has been found. InSb epilayers grown on InSb substrate after the above oxide desorption exhibited x-ray rocking curve with full width half maxima of 13 arc-sec, reproducibly.

Efforts of our research have also been devoted to aspects of material characterization. Low temperature photoreflectance (PR) of Te- doped GaSb has been used to determine the transition energy of spin-orbit split component of the fundamental band gap. Temperature dependence of this transition energy has been determined. These are the first PR reports on GaSb.

Theoretical calculations of a novel InAsSb/InTlSb superlattice structure lattice-matched to InSb indicated a type I band alignment, with optical band gap in the long-wavelength region.

14. SUBJECT TERMS

Molecular Beam Epitaxy, Photoreflectance,
Semicondcutor Materials

15. NUMBER OF PAGES
47

16. PRICE CODE

17. SECURITY CLASSIFICATION OF REPORT	18. SECURITY CLASSIFICATION OF THIS PAGE	19. SECURITY CLASSIFICATION OF ABSTRACT	20. LIMITATION OF ABSTRACT
Unclassified	Unclassified	Unclassified	

TABLE OF CONTENTS

Grant# F46920-93-1-0111DEF, funded for $580,002 from 1/15/93-3/14/97
Project Title: MBE Growth of GaInAsSb

This is a final technical report describing the research activities of the above AFOSR grant. The three year grant period began on Jan.15, 1993 and was extended on a no-cost basis for a year and two months up to March 14, 1997. This program involved the effort of two faculty members, one Research Associate, seven graduate students (one Ph.D. candidate, six MSEE students/candidates) and three undergraduate students. Amongst these are three minority /female graduate students and two minority and female graduate students. During this period, there has also been collaborative efforts with other institutions. Ms. Audra Rice, a graduate student from Dr. Kevin Malloy's group at University of New Mexico, carried out the low temperature Hall measurements on numerous MBE grown samples. Close collaboration with Dr. Mitchel's group at Wright Laboratories, WPAFB, which began in summer of 1991, has been continuing. Low temperature photoluminescence (PL) measurements were carried out by Dr. S. Hegde and low temperature Hall measurements were also carried out by Dr. W. Mitchel. His suggestions were helpful in setting up low temperature Hall measurements in our laboratory at North Carolina A&T State University. Collaboration with Dr. K.K. Bajaj, a well known theoretician from Emory University, which also began in 1991 is continuing. These collaborations were very fruitful and permitted rapid advances outlined in this report. During this entire grant period, the suggestions of technical monitor Major Mike Prairie were extremely helpful.

I. OBJECTIVES

The goal of this project was is to investigate semiconductor materials for applications in the mid and long wavelength IR region, particularly in the atmospheric IR transmission windows (3-5 and 8-12 μm) for IR counter measures and IR radar for aircraft & automobiles. This spectral band is of considerable importance to Defense due to the tactical and strategic advantages that it provides such as night vision, navigation, flight control and early warning systems, which require the availablility of high performance detector arrays. The original objectives of this research program were to set up the MBE system, growth of GaInAsSb epilayers and investigation of their physical properties for long wavelength opto-electronic device applications. The tasks proposed in the original proposal were modified throughout the grant period, with the consent of the technical monitor, in order to facilitate proper calibration of the system and to establish the in-house characterization for these materials. Hence, the major thrusts in the research work carried out during this period were slightly different, though the main goal was the same. The work carried out can be broadly classified into the following categories.

- MBE system, which was acquired in June 1995 from the funding obtained from another AFOSR equipment grant (Grant # F49620-93-1-0540DEF), was calibrated and optimized in terms of the substrate temperature, source fluxes and the growth of

epilayers of binary compounds GaAs, GaSb and InSb. MBE growth of homoepitaxial InSb epilayers and its oxide desorption have been the subject of detailed investigation. Growth of quaternary GaInAsSb layer has also been demonstrated.

- Theoretical investigations on a InTlSb/InAsSb superlattice lattice matched to InSb was carried out. It has been shown that this structure has potential application for the long wavelength detectors in the 8-12 μm wavelength region. This structure may offer an advantage over the InTlSb epilayers' in terms of the structural quality as it will be sandwiched between high quality zincblende InAsSb epilayers.
- Efforts of our research were also directed towards the characterization of Liquid Phase Electroepitaxially (LPEE) grown layers using photoreflectance technique. Room temperature photoreflectance(PR) was set-up in the previous grant (Grant No. F49620-89-C-0004) supported by AFOSR. The set-up was extended to low temperature up to 4K using closed cycle cryogenic system. The information obtained from these layers would serve as a guideline in determining the quality of the MBE grown epilayers and in future could also become an integral part of the MBE system, serving as an in-situ characterization tool. Low temperature photoreflectance of LPEE grown GaSb samples was carried out in the energy range of 1.3 to 1.8 eV encompassing spin orbit split component of the fundamental band gap ($E_0+\Delta_0$). Temperature induced shift in these transitions was also investigated.
- Existing Hall measurement equipment was restored and upgraded for higher accuracy over 10 K to 400 K range and B field ranges from 10 to 6 KG, to accommodate narrow bandgap III-V materials. The Hall and resistivity data on MBE grown Sb based compounds were verified by comparing the values obtained by other labs on the same samples.

II. MAJOR ACCOMPLISHMENTS

- MBE system, which was delivered in June 1995, had quite a few major problems, most of which have been solved. The vacuum of the growth chamber routinely reaches 1 to $2x10^{-10}$ torr during Sb-based material growth and 10^{-11} torr under idle cell condition. This is achieved without the use of sublimation pump attached to the 400 l/s ion pump.
- Growth of GaAs on GaAs substrate with specular surface and oval defect density less than 200/cm^2 has been achieved. The best full width half maxima of the x-ray rocking curve for (400) peak achieved on both 1μm and 10 μm thick MBE grown GaAs layers is 15 arc-sec.
- Growth of GaSb on GaAs (100) substrates with room temperature carrier concentrations in the low and mid 10^{16}/cm^3 range and mobility in the range of 200-450 cm^2/V-sec ,which increased to 3500-4000 cm^2/V-sec at 77K with a background carrier concentration of 10^{14}/cm^3 have been accomplished. The low temperature PL indicated half width of 3 meV for DA transition at 713 meV attesting to the good quality of the grown epilayers.
- A new and expeditious method for thermal desorption of oxide from InSb substrate has been proposed that allowed reproducible homoepitaxial growth of the epilayer with x-ray FWHM of 13 arc-sec.

- Low temperature PR signal on Te doped bulk and Liquid Phase Electroepitaxially (LPEE) grown GaSb layers corresponding to $E_0+\Delta_0$ critical points has been obtained. The temperature dependence of this transition point has been determined and these we believe are the first observations of the PR signals as well as the temperature induced shifts in GaSb.
- A novel superlattice (SL) heterostructure, comprising of InTlSb well and InAsSb barrier lattice matched to InSb, is proposed for long wavelength 8-12 μm detectors. Preliminary energy band calculations of 30Å $InAs_{0.07}Sb_{0.93}$/100Å $In_{0.93}Tl_{0.07}Sb$ SL show the band alignment favorable to type I with three heavy-hole subband confinement in the valence band and a partial electron subband confinement in the conduction band due to the small conduction band offset.

III. MBE SYSTEM

A. CALIBRATION OF THE SUBSTRATE TEMPERATURE

The first step prior to the growth of GaAs was to calibrate the substrate temperature and the vapor pressures of the Ga and As. Measurements of the substrate temperature, one of the critical growth parameters, were done using a thermocouple, which was either in contact with a molybdenum block (in the case of indium soldered substrates), or a heat diffuser (in the case of the indium free substrate mounts). In both cases the thermocouple readings were calibrated from the RHEED or the changes in surface morphologies. These are GaAs oxide desorptions at 580-610 ^{0}C, surface topography modification of Al/Si eutectic melting point at 577 ^{0}C and (1x3) to (1x5) reconstruction change at temperature of 400 +/- 20 ^{0}C on Sb stabilized GaSb surface, as described below.

(a) Oxide desorption on GaAs at 580-610 ^{0}C

Oxide desorption on GaAs surface has been reported [1,2] to be around 580-610 ^{0}C. The oxide deposition on a 1x2 cm wafer was monitored using RHEED. The observed oxide desorption temperature was influenced by the substrate preparation, duration of heating, ramping and the growth chamber environment. Initially we established the duration it takes for the Mo block to stabilize after the readings of the Eurotherm temperature controller became steady. The surface temperature was determined using the pyrometer. It was found that once the thermocouple reading reached the set value and stabilized within ~0.1 °C, the surface temperature took another couple of minutes to stabilize. Therefore, near the desired substrate temperature of desorption, T_s, the temperature was incremented in the steps of 5 to 10 °C and surface temperature of the Mo block was allowed to stabilize after each increment. Duration of heating of the substrate was minimized this way. It was noticed that the oxide desorption temperature was measured to be higher when the system was fairly new. However, with deposition of GaAs over a period of time, the emissivity of the Mo block changed and the oxide desorption temperature became more steady after a few growth runs. Eurotherm temperature controller settings for the desorption temperature differed slightly with each Mo block as shown in the Table I. As pressure was found to have significant influence on the oxide desorption temperature by as much as 30 °C. Hence, the oxide desorption

temperature was determined under the conditions of less As pressure and the substrate temperature was calibrated assuming the oxide desorption temperature to occur at 580 °C.

TABLE I: Eurotherm temperature controller setting T_s, and the pyrometer reading, T_p, for the GaAs oxide desorption temperature (assumed to be at 580 °C) for different Mo blocks and different growth runs.

Mo. Block #1:

Sample #	426	508	513	722	726	806
T_s(°C)	780	740	745	740	725	700
T_p(°C)	564	537	545		554	532

Mo. Block #2:

Sample #	429	506	605	719	730	812
T_s(°C)	770	770	770	730	720	730
T_p(°C)	560	558	558	550	541	545

Mo. Block #3:

Sample #	430	503	514
T_s(°C)	750	760	760
T_p(°C)	561	556	556

(b) Surface morphology alteration at Al/Si eutectic melting point

Al layer of about several hundreds nm was deposited on Si at room temperature in the MBE growth chamber. The change in the surface morphology was observed through a telescope on raising the substrate temperature. Mo block #3 was used. The substrate temperature was ramped very slowly (~1° C/minute) when it was closer to the eutectic temperature of 577 °C. The surface smoothness changed drastically at the temperature controller setting of 745 °C which has been taken to correspond to the substrate temperature of 577 °C.

(c) Surface reconstruction change on GaSb surface

It has been reported in the literature[3] that Sb stabilized GaSb (100) surface exhibits (1x3) reconstruction for temperatures above 400 °C and (1x5) reconstruction below 400 °C and the transition temperature is around 400 °C. In order to observe this, GaSb films were grown at a growth temperature of 500 °C. (1x3) surface reconstruction was observed on the RHEED pattern. The substrate temperature was decreased with Sb source flux "on" to ensure a Sb-stabilized surface. Temperatures at which the surface reconstruction change occurred was assumed to be at the substrate temperature of 400 °C

(see Table II). This reconstruction change was found to be very sensitive to temperature , however, relatively insensitive to Sb flux intensity.

TABLE II: Surface reconstruction change on Sb stabilized surface for samples on different Mo blocks.

Mo. block	#1	#2	#1
Sample#	722	719	726
T_S (°C)	590	585	595
T_p(°C)	410	408	415

Figure 1 shows the substrate temperature calibration chart that has been constructed based on the experimental data determined from al l the above three methods, which is being used currently to set the desired substrate temperature. The difference between the thermocouple reading and actual surface temperature as determined by above three methods varied from ~145 °C to ~190 °C.

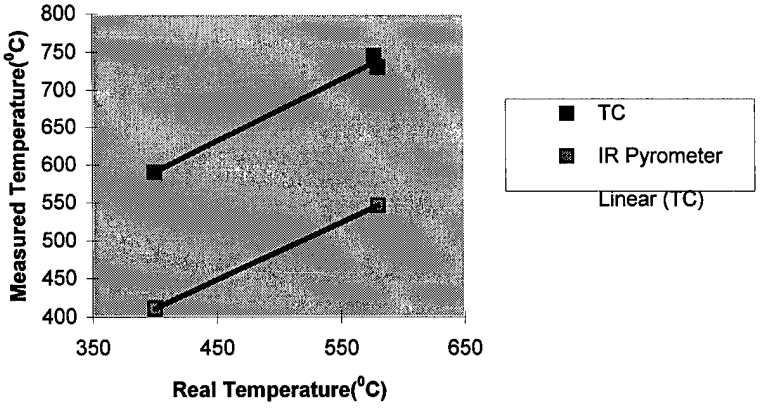

Fig.1. Calibration curve for the substrate temperature.

B. CALIBRATION AND REPRODUCIBILITY OF THE SOURCE FLUXES

Table III tabulates the source fluxes that were calibrated using the flux monitor. For the calibration of group V fluxes, the flux monitor was saturated with group V flux prior to commencement of the calibration procedure as a large transient is observed on changing the fluxes from group III to group V. The reproducibility of source flux from run to run was also examined. Ga flux exhibited the best reproducibility within 6% , with Sb flux being the worst at 20%, respectively.

TABLE III: Measurements of source fluxes using flux monitor for various growth runs. Cell temperature (Tc) for different cells are also indicated.

Growth run		1	2	3	4	5	6	7	8	9
Ga	T_c(°C)	1170	1170	1170	1170	1170	1170	1170	1170	1170
	flux(10^{-7} torr)	2.80	2.84	2.80	2.96	3.05	2.80	3.00	3.00	2.85
As	T_c(°C)	350	350	350	350	350	350	350	350	
	valve(mil)		100	100	140	110	100	95	90	90
	flux(10^{-6} torr)		1.5	1.34	2.5	1.68	1.6	1.2	1.0	0.62
Sb	T_c(°C)		560	560	560	560				
	flux(10^{-7} torr)		10.2	9.5	8.4	8.3				

We also attempted to calibrate the As flux intensity as a function of the valve position (Table IV). The flux intensity seems to exhibit a linear variation with the valve position in a single run, however the reproducibility from run to run has been poor.

TABLE IV: Calibration of the As valved cracker source indicating the valve performance. As bulk and tip zones were held at 350 °C and 600 °C, respectively.

Valve(mil)	0	40	100	150	110	100	90	100	100
Flux(10^{-7} torr)	0.01	1.3	11	24	15	13	8.4	8	8.5

C. PROBLEMS ENCOUNTERED WITH THE MBE SYSTEM

As with any new MBE system, after loading source materials into the MBE chamber and initiating crystal growth, several serious problems were encountered with the system, most of which have been solved. A few of these are listed below.

(a) *Flux monitor*

The ion gauge provided by EPI was extremely unstable resulting in inaccurate and irreproducible flux measurement. This rendered considerable impediment to the progress of the research due to the inability to establish the experimental parameters. The entire flux monitor assembly was disassembled and sent back to EPI for repair. However they were unable to find the source of the problem. After reinstallation into the MBE chamber during the early part of this year, the stability of flux reading has been better, though not completely normal. The problem appears to be associated with the design of the EPI monitor. The EPI flux monitor installed in other MBE systems has also been reported to exhibit similar problem.

(b) *RHEED system*

Considerable problem was also encountered with RHEED over a long period. VG Fison's LEG110 RHEED did not function properly and had to be returned to the factory at UK . The vendor took six months to repair. Further, it was found that the RHEED was located between the two ion pumps for the growth and buffer chamber. Hence, there was significant magnetic field (~5G), which caused the electron beam to deflect. Hence, a suitable magnetic shelter was designed to minimize the magnetic field.

(c) *Water manifold*

In EPI MBE system, the As, Sb crackers, substrate heating stage, two Ti-sublimation pumps and the turbo pump are cooled by water. The water connection for As, Sb and substrate heating stage is connected in series. With time the cooling for these three items was found to deteriorate. As the water manifold was made of Al, the latter reacts with water forming aluminum oxide, eventually blocking the water flow in the manifold. This problem was alleviated by replacing it with a brass water manifold. Other minor changes were made to accomplish efficient cooling such as separating the cooling lines of the manipulator from the cracker furnaces , addition of a manual valve to the cooling lines of the vacuum pumps that is normally closed during the growth, and changing the quick connection to compression tube fittings.

(d) *Vacuum in the buffer chamber*

Since the installation of the system, leak in the buffer chamber was suspected due to the low vacuum of 10^{-8} torr observed in this chamber. Leak spot was located on the water cooling tubing inside the ion pump that provides cooling for the Ti-sublimation pump. As normally the tubing is filled with water, this leak detection was found to be the most challenging one. The entire sublimation unit was sent to the manufacturer to rebuild the unit and the port on the ion pump was blanked with an eight inch CF flange. The pump has been reinstalled and vacuum of $7x10^{-11}$ torr is routinely achieved in this chamber.

(e) *Source cells*

Two source cells that caused considerable problems were Al and Sb. Heating filament in the Al cell was shorted due to the Al climbing along the crucible wall due to

the faulty filament cell design. EPI modified the cell design suitable for a cold lip crucible. Erratic changes in the Sb cracker zone temperature occurred due to the frequent shorting of the thermocouple and the filament. This has been traced to Sb flakes falling from the chamber into the cell. There is a considerable Sb build up around the radial vane cooling shelter due to the chamber design. This problem can probably be minimized by changing the cell position to the upper quadrant and plan to do at a later time when the chamber is opened.

(f) *Oval defects*

Examination of the surface morphology of MBE grown GaAs by Nomarski phase contrast microscope revealed a high oval defect density of $10^4/cm^2$. The reasons for these are well documented in literature and has been commonly attributed to either Ga cell spilling and/or oxidized Ga source. The problem persisted even after several growth runs, and seemed to be independent of the growth temperature (GaAs were grown at 600 °C for this purpose) and As/Ga beam equivalent pressure (BEP) ratio. Initial sample heating prior to the growth did not result in significant difference. All the cells to be used for the growth were heated one day earlier to the growth run and this resulted in the reduction of the oval defect density to $1,400/cm^2$. The cleanliness of the substrate during the loading appears to be the major problem. GaAs layer with specular surface and oval defect density less than $200/cm^2$ has been successfully grown.

D. CURRENT STATUS OF THE MBE SYSTEM

(a) Substrate temperature

With time the measurement of the substrate temperature using the thermocouple and IR pyrometer reading has reached a stable and reproducible condition. The difference between the two readings has reduced from 180 °C to 145 °C as shown in Fig. 2. This is caused by material coating of the MBE chamber, substrate heating stage, and Mo blocks, resulting in the saturation of the emissivity.

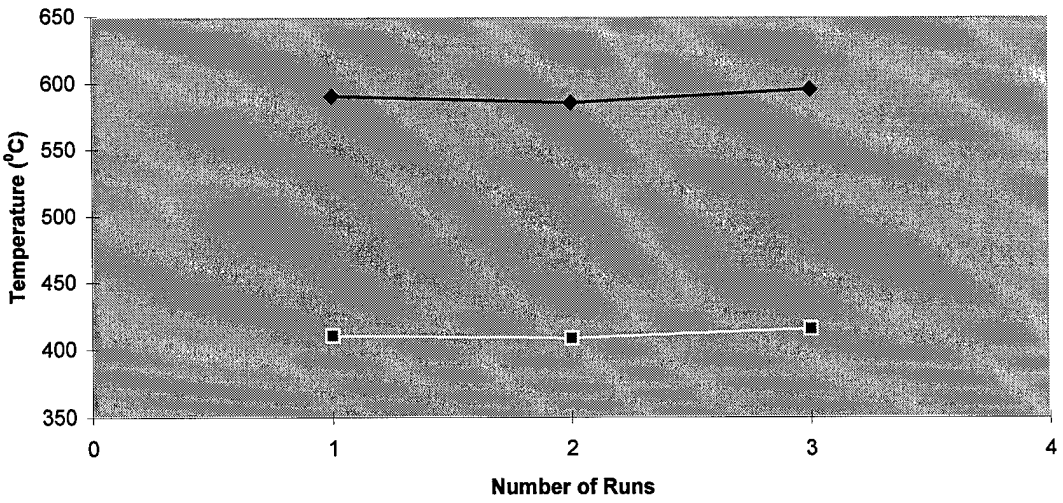

Fig.2. The substrate temperature at which the surface reconstruction phase of GaSb (001) changes from (3x1) to (5x1) under Sb stabilized condition for different growth runs. The lower and higher temperatures correspond to the pyrometer and thermocouple reading, respectively.

(b) Vacuum

The vacuum of the growth chamber routinely reaches 1 to $2x10^{-10}$ torr during Sb-based material growth and 10^{-11} torr is achieved when all cells are at idle condition. This is achieved without the use of sublimation pump attached to the 400 l/s ion pump.

(c) Source flux performance

All the group III source flux are stable and reproducible. There was problem with the stability and reproducibility of the Sb flux. When the MBE system was opened, the baffle in the cracker zone of the Sb cell was removed, and since then the Sb cracker is operated at higher temperatures. This has resulted in an improved performance in terms of the flux stability and reproducibility. Amongst all the PID setting, the ones for the Sb cell was found to the most challenging one. It appears to have a very narrow window for optimizing the cell performance. A minor variation in this causes considerable instability in the performance of the cell. Figures 3 and 4 depict the variation in In and Sb flux with cell temperatures, respectively. The data was taken over several growth runs.

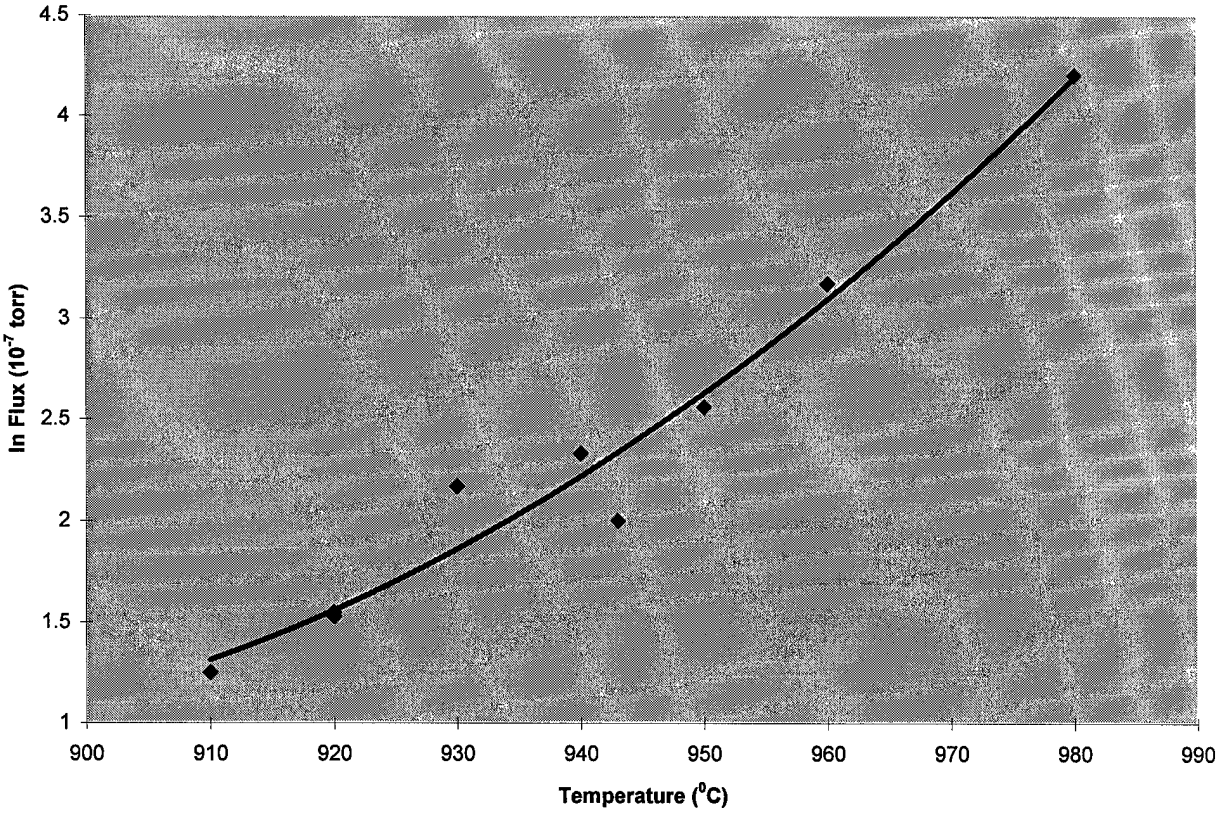

Fig.3. The In beam source flux as a function of cell temperature. The data are collected from different growth runs.

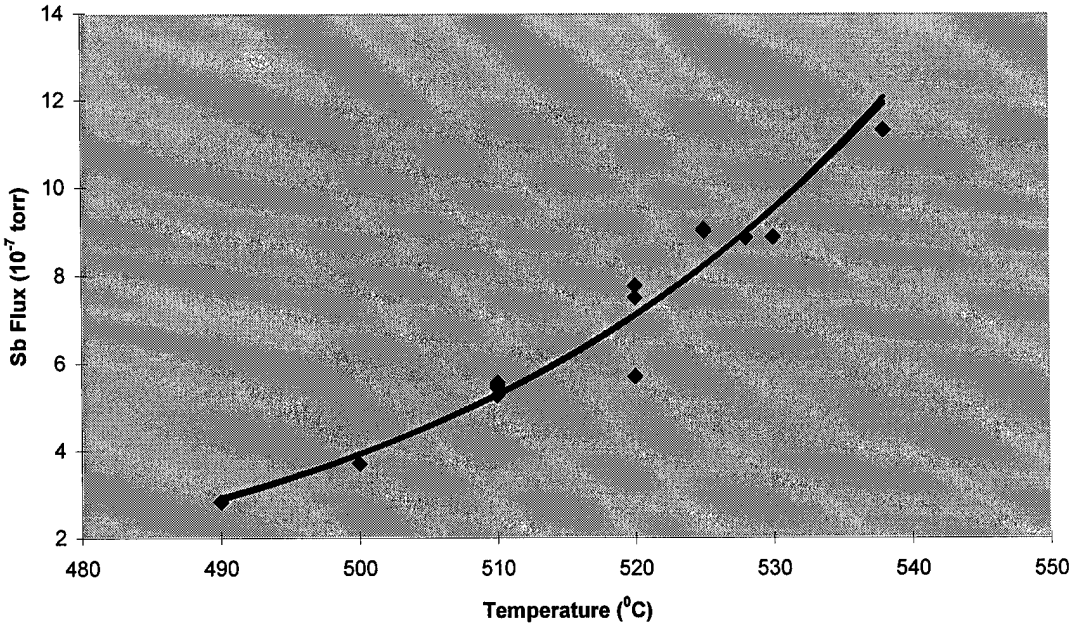

Fig.4. The Sb beam source beam flux as function of cell temperature. The data are gathered from different growth runs.

E. PURCHASE AND INSTALLATION OF RHEED IMAGE ACQUISITION SYSTEM

Reflection high energy electron diffraction is the most powerful tool to carry in situ growth monitoring and analysis in MBE. RHEED images provide considerable information on growth kinetics, surface and crystalline quality. Our recent purchase of RHEED Image Acquisition and Analysis system from K-space, extends significantly the capability of our system. This was acquired under another subcontract (F49620-95-1-05) the original sponsor being AFOSR.

The hardware part of the system consists of CCD camera, mounting frame, image card, while the software comprises of KSA400 developed by K-space Inc. for RHEED image data acquisition and analysis. The capabilities include the measurements of RHEED intensity oscillation, surface lattice spacing, surface coherent length, single image and multiple image recording, window analysis, time logging of intensity anywhere on a RHEED image, time logging of the width of RHEED streaks and the spacing between the streaks, and can be interlocked with MBE control system to perform phase-lock epitaxy.

IV. MBE GROWTH

A. GROWTH OF GaAs EPILAYERS

The MBE growth of GaAs layer was carried out at a growth temperature of 580 $^{\circ}$C at a background pressure of ~7×10^{-10} torr. Figure 5 illustrates the variation of the FWHM of x-ray rocking curve as a function of As to Ga BEP ratio at a growth temperature of 580 $^{\circ}$C. The crystalline quality starts to degrade once the flux ratio goes below 4:1. The

optimized As to Ga flux ratio was found to be ~ 4:1, close to stoichiometric condition. This is consistent with the reports in the literature and has been attributed to the accumulation of Ga at the surface, due to its low vapor pressure, and reevaporation of As due to its high vapor pressure, thus making growth relatively insensitive to the As overpressure. In the recently grown samples, FWHM of x-ray rocking curve as low as 15-17 arcsec was obtained.

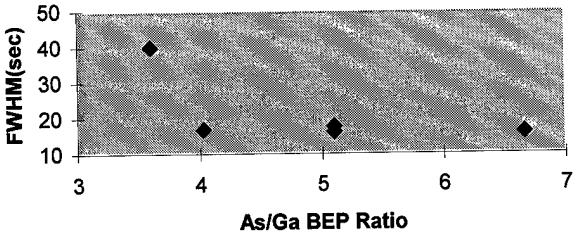

Fig.5. Variation in FWHM of x-ray rocking curve of GaAs epilayers with As/Ga BEP ratio.

TABLE V: Summary of GaAs growth and characterization data.

Sample	426	429	430	503	806	812
Mo. block	#1	#2	#3	#3	#1	#2
T_s(°C)	770	764	750	760	700	710
T_p(°C)	556	552	556	552	530	527
T_{Ga}(°C)	1170	1170	1170	1170	1150	1170
$f_{Ga}(10^{-7})$:						
bf gro	3.0	3.15	3.05	3.0	2.7	3.5
af gro	2.8	2.98	2.8	3.0		3.4
T_{As}(°C)	350	350	350	350	350	370
V_{As}(mil)	110	100	95	90	115	82
$f_{As}(10^{-6})$:						
bf gro	1.68	1.6	1.23	1.0	1.02	2.33
af gro	2.2	1.65	1.34	1.16	1.13	2.0
f_{As}/f_{Ga}	5.6	5.1	4.03	3.33	5.1	6.66
Growth Time(h)	2.1	2.0	3.28	0.3	2.67	2.08
RHEED	2x4	f2x4	f2x4	v4x2	w2x4	w2x4
FWHM, x-ray(sec.)	44	16.1	16.8	X	17.5	16

Sample	906	909	911	912	917	918	920	923	925
T_s(°C)	740	740	757	757	775	772	775	775	775
T_p(°C)	543	541	553	559	560	562	562	565	568
T_{Ga}(°C)	1125	1125	1125	1125	1125	1125	1125	1125	1125
$f_{Ga}(10^{-7})$:	2.08	2.15	2.14	2.14	2.08	2.15	2.21	2.12	2.14
T_{As}(°C)	370	370	370	370	370	370	370	370	370
V_{As}(mil)	50	70	70	70	80	70	90	95	100
$f_{As}(10^{-6})$:	1.09	1.47	1.47	1.47	1.70	1.40	1.87	2.22	2.22
GT(h)	2	2.25	1.33	2.5	2.67	2.2	2.2	8	7.8
RHEED	f4x2	w2x4	w2x4	w2x4	2x4	w2x4	b2x4	b2x4	b2x4
X-ray FWHM(arc-sec)	21	17.4	18.5	17.4	15.3	28	15.7	23	15

w- weak, b-bright, bf gro- before growth, af gro- after growth

B. GROWTH OF GaSb EPILAYERS

GaSb layers have also been grown on GaAs(100) substrate. The growth parameters had to be more stringently controlled than in the case of GaAs layers, in order to obtain good quality layers. The typical growth rates are ~1μm/hour. Low temperature (4.5K) PL on the MBE grown GaSb layers indicated a full width half maxima of 3 meV.

The base pressure during the GaSb growth was $4x10^{-10}$ torr. Figure 6 depicts the variation of the FWHM of x-ray rocking curve of MBE grown GaSb films as a function of Sb to Ga BEP ratio at a growth temperature of 500 °C. The best crystalline quality of the epilayers was achieved for a BEP ratio in the range of 3.5 to 4. Bright RHEED patterns with (1x3) reconstruction corresponding to Sb stabilized pattern were observed, indicating Sb rich growth condition. On a 1.5 μm thick film, a FWHM of 102 arc-seconds for (400) peak has been observed, which compares well with the reported values in literature on good quality layers. The typical growth rate of GaSb is 1 μm/hr (Table VI). For the flux ratio below 3.5, there was considerable degradation in the quality of the layers often resulting in polycrystalline or amorphous layers. On increasing the BEP ratio beyond 4.0, the crystalline quality again became worse, though layer remained single crystalline.

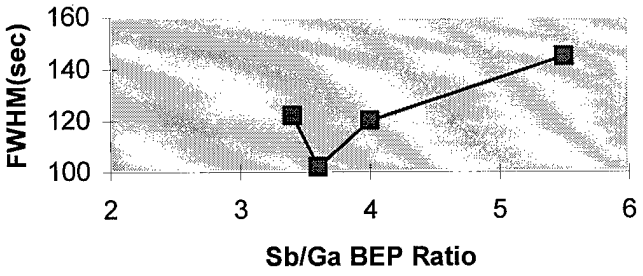

Fig.6. FWHM of x-ray rocking curve of GaSb epilayers as a function of Sb/Ga BEP ratio.

TABLE VI: Summary of GaSb epilayer growth and characterization data.

Sample	506	508	513	514	605	719	722	726	730
Mo. blk	#2	#1	#1	#3	#2	#2	#1	#1	#2
T_s(°C)	650	645	640	630	640	630	660	660	660
T_p(°C)	460	460	451	450	465	462	480	495	485
T_{Ga} (°C)	1170	1170	1170	1170	1170	1150	1150	1150	1150
$f_{Ga}(10^{-7})$:									
bf gro				2.8	3.1	2.1	2.05	2.02	2.1
af gro	3.16	2.84	2.76						
T_{Sb}(°C)	528	536	560	550	560	560	560	570	560
$f_{Sb}(10^{-7})$:									
bf gro	6.61	7.5	14.1	7.0	10	8.4	8.3	10.6	12.5
af gro	5.8	7.0	10.0		9.0			14.0	11.0
f_{Sb}/f_{Ga}	1.85	2.6	3.6	2.5	2.9	4.0	4.05	5.5	5.9
Growth rate (μm/h)			1.45			1.17	0.96	1.04	1.15
Growth time (h)			4.13			3.77	4.17	3.85	4.35
RHEED			1x3			1x3	1x3	b1x3	b1x3
x-ray(s.)			102			120	418	145	125
				p	p	p	p		
μ(cm^2/Vs)@RT				455		215		452	430
@ 77K				3540		125		3582	2480
p (cm^{-3}))@RT				$2.6x10^{16}$		$5.6 x10^{16}$		$1.6x10^{16}$	$7.1x10^{16}$
@ 77K				$5.6 x10^{15}$		$2.4 x10^{16}$		$2.3x10^{15}$	$3.9x10^{15}$

Figure 7 is the dependence of GaSb growth rate on the Ga flux intensity. As Ga sticking coefficient is unity at 500 °C, the growth rate is primarily determined by the Ga source flux intensity. In the absence of RHEED oscillation system this data may serve as a calibration parameter to control growth thickness.

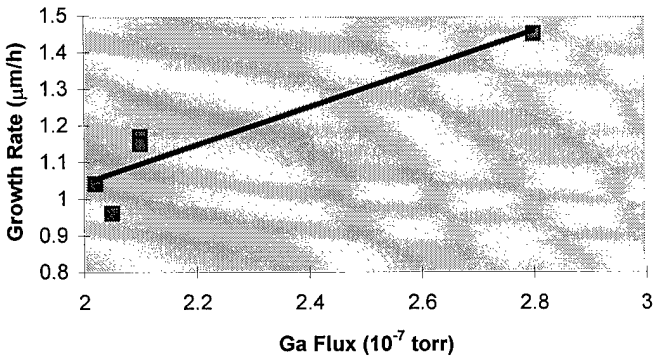

Fig.7. Growth rate of GaSb vs Ga flux.

(a) *Hall data*

The electrical characteristics of these layers grown on GaSb were investigated. Hall measurements indicated strong freeze out of free carriers from $8x10^{16}$ to $3x10^{16}/cm^3$ as the temperature decreased from 300 K to 77 K indicating the presence of deep acceptors as shown in Fig. 8. The mobility at 77 K were in the range of 3,000-4,000 cm^2/V-sec on these samples. (see Fig. 9)

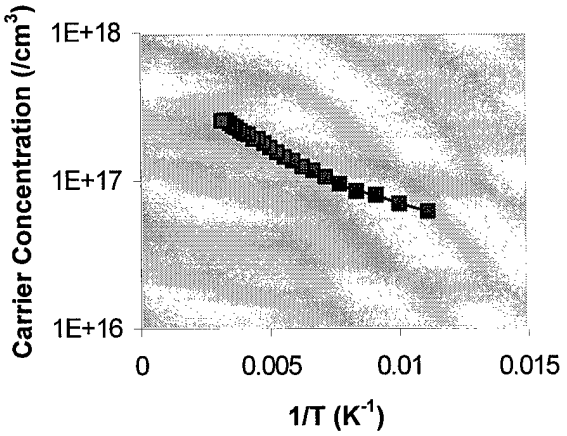

Fig.8. Temperature dependence of carrier concentration in GaSb epilayers.

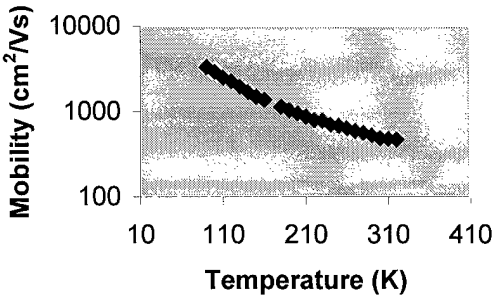

Fig.9. Temperature dependence of mobility in GaSb epilayers.s

(b) *PL data*

Figure 10 illustrates the PL spectra at 4 K for GaSb grown on GaSb substrates. High energy transitions at 807 meV and 808.4 meV are associated with an unidentified and exciton bound to the native acceptor level at 34 meV, respectively. The band to acceptor transition at 777.5 meV is also observed in all the layers. In few of the layers, an additional sharp peak at 767 meV is observed, probably due to an exciton bound to the doubly ionized acceptor while in others a broad peak at this energy is observed. The origin of this peak is not clear. In the GaSb layer grown on GaAs only one peak corresponding to 779.5 meV is observed. This is attributed to the band or donor to acceptor transition, shifted due to the strain associated with the layer.

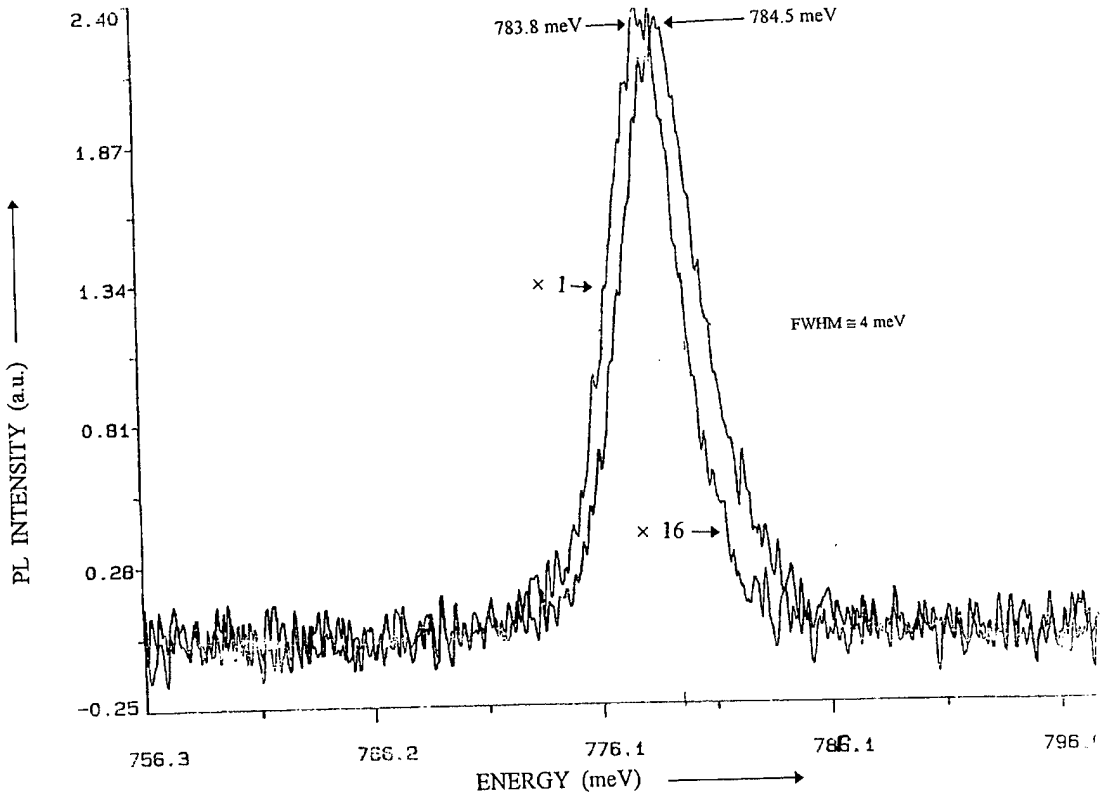

Fig.10. 4K PL spectra of GaSb on GaAs

C. GROWTH OF InSb EPILAYERS

Initially the aim of the work on InSb growth was to calibrate our system. However, the excellent quality of the homoepitaxial layer of InSb led us to a somewhat more detailed research on this system than the one that we had originally planned for. InSb substrate preparation has been reported to be the most challenging one amongst the III-V semiconductors due to the presence of native oxide. The comparable vapor pressure of indium oxide with that of InSb has made the desorption of the former a formidable task.

Various techniques have been reported in literature [4-6] to solve this oxide problem which include in-situ ion etching and a combination of ex- situ chemical etching with thermal desorption under Sb flux. The first technique calls for in-situ ion etching facilities, which is not present in most of the system. Hence, the second technique has been one of the extensively investigated procedure. So far it has gained only limited success as it takes few hours to complete the oxide desorption. Our work indicated that the sequence of Sb introduction into the system is critical to the desorption of oxide. We carried out a detailed investigation of the in-situ preparation of the substrate and the combination of ex- and in-situ preparation of the substrates as discussed below.

(a) Ex-situ preparation of InSb(001) substrate

Three different ex-situ treatments of InSb substrate were investigated. They are (1) standard degreasing process without etching, (2) etching with bromine-methanol and (3) etching with lactic acid, HNO_3 and HCl solution of composition 25:4:1 for 90 seconds at room temperature. It was found that the third procedure gave the smoothest surface after oxide desorption in terms of bright and streaky RHEED patterns as illustrated in Figs. 11(a)- (c).

(a)

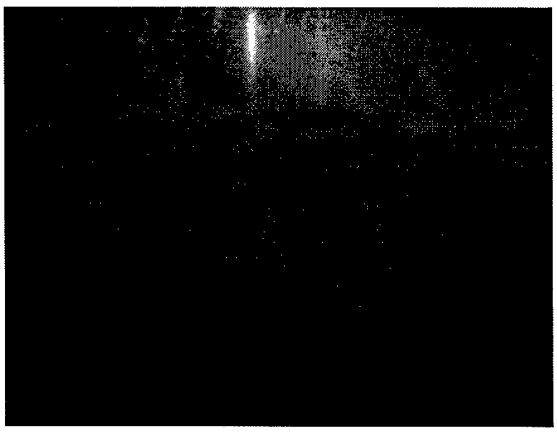

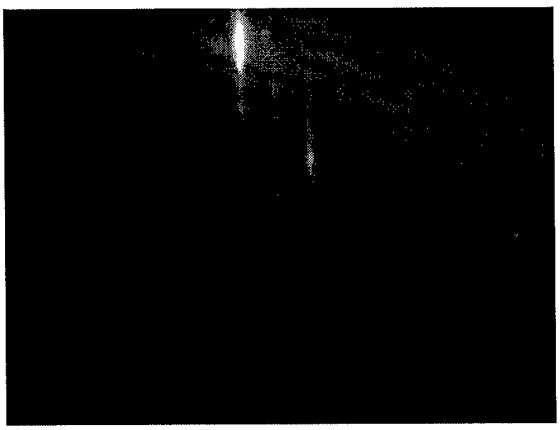

(b)

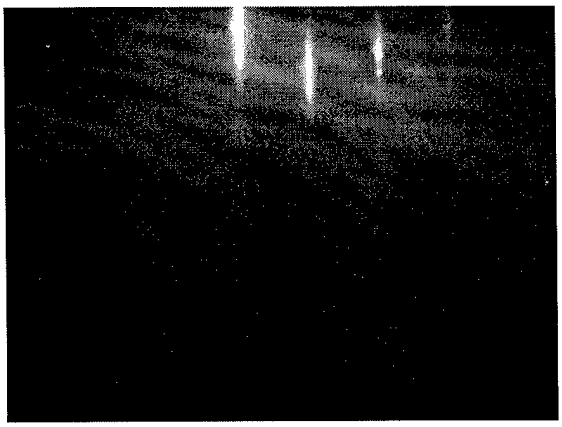

(c)

Fig.11. RHEED image after oxide desorption for (a) InSb substrate without etching, (b) etching with bromine methanol solution and (c) etching with lactic acid: HNO_3 : HCl.

(b) *In- situ thermal treatment of InSb substrate*

Four different in-situ procedures for oxide desorption process were examined. These were desorption (1) under Sb flux from room temperature, (2) in the absence of Sb flux, (3) introduction of Sb flux only at elevated substrate temperature but prior to oxide desorption and (4) introduction of Sb flux immediately after oxide desorption.

The first treatment produced rough surface as observed by Nomarski phase contrast microscope. RHEED image of such surfaces exhibited polycrystalline rings in addition to InSb diffraction pattern. These polycrystalline rings increased in number with increase in the Sb flux intensity as shown in the RHEED images (Figs. 12(a) and (b)). It

was found that once the rings are formed they could not be eliminated under any condition. InSb homoepitaxy grown on this surface exhibited poor crystalline quality as determined by high resolution x-ray diffraction. The full width half maxima (FWHM) of the x-ray rocking curve obtained on these layers is around 40 arc-sec as depicted in Fig. 13.

The second treatment resulted in considerable indium dots though otherwise exhibiting smooth surface as shown in Fig. 13(b). RHEED image exhibited bright and streaky diffraction pattern of InSb.

The third treatment also yielded rough surface. On opening the Sb flux below 320 °C, polycrystalline rings were observed in the RHEED image as in the first case. However, when Sb flux was introduced above T_s=320°C, two stages of oxide desorption were observed as reported in the literature [4,7]. The first stage involved the desorption of antimony oxide at 440°C. RHEED image exhibited two diffraction patterns superimposed on each other (Figs. 13 (c) and (d)). The streaky pattern corresponded to the InSb substrate while the broken lines have been attributed to In_2O_3 , as the surface lattice dimension of this additional diffraction pattern (Fig. 13(b)) was closely matched to that of In_2O_3(a_0=10.12 A°)[8]. This measurement was done using K-space RHEED image data acquisition - analysis system and calibration was done against the diffraction streaks of InSb substrate. The intensity of this additional diffraction pattern

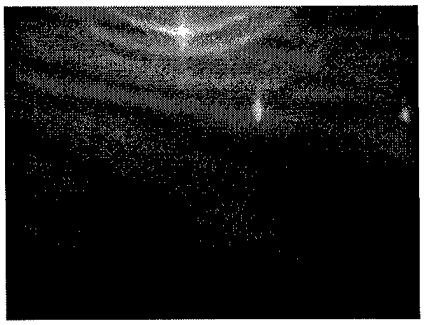

(a)

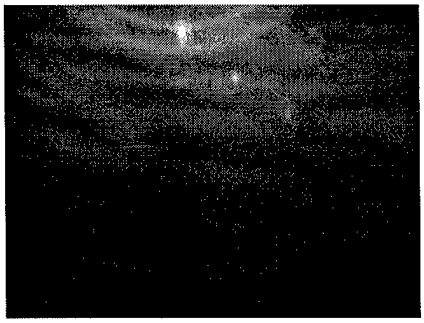

(b)

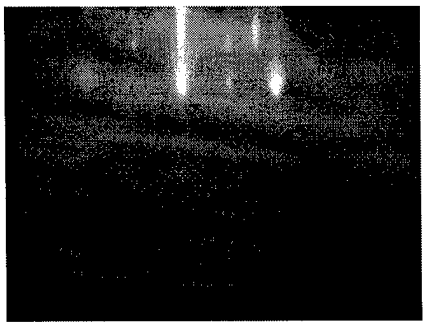

(c)

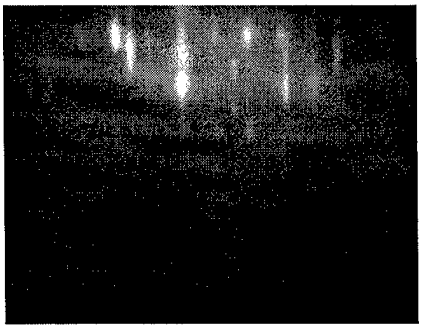

(d)

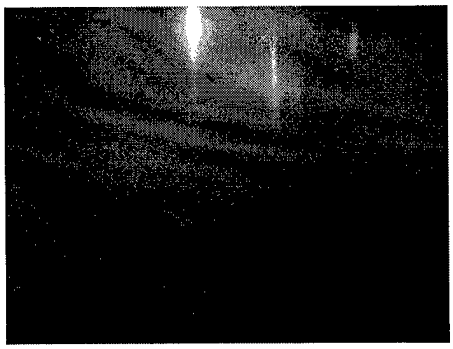

(e)

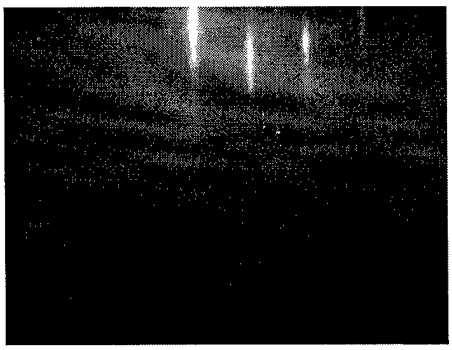

(f)

Figure 12. RHEED images (a), (c) and (e) are taken along <100> azimuth, (b), (d) and (f) along <110> azimuth. (a) and (b) are images after the treatment 1 oxide desorption process, e.g., Sb flux was open from room temperature and throughout the entire desorption process. Presence of polycrystalline rings in addition to the InSb diffraction pattern is clearly evident. Images (c) and (d) correspond to the case after treatment 3, e.g., Sb flux open at temperatures above 320°C but prior to oxide desorption. Additional diffraction pattern observed has been attributed to the presence of In_2O_3. Images (e) and (f) are taken after treatment 4 with Sb flux open only after oxide desorption at 440°C. Only diffraction pattern corresponding to InSb is observed.

can be reduced and eventually be eliminated on heating the substrate to 490°C for extended period of time (hours). A similar observation has been reported in literature [4-7]. Further, it was found that the formation of In dots could be prevented by maintaining Sb flux above a certain value. The surface so obtained was mirror smooth. However, FWHM of the x-ray rocking curve was broad, as shown in Fig. 13, for InSb films grown on the surface that had additional RHEED diffraction pattern.

The best results were achieved using the fourth treatment. Prior to the thermal treatment the surface was amorphous, as indicated by RHEED, which was replaced by the bright RHEED pattern (Figs. 12(e) and (f)) on increasing the substrate temperature to 440°C in the absence of Sb flux. No other polycrystalline rings or any other diffraction patterns were observed as in the rest of the above three cases. These observations suggest the complete desorption of oxide from the InSb surface using this technique. On introducing Sb flux and maintaining the substrate at elevated temperatures of 440-460°C for few minutes, yielded mirror smooth surface with no In dots. Homoepitaxial growth of InSb epilayers on this surface produced epilayers of superior structural quality, as exhibited by the narrow FWHM of around 14 arc-sec obtained on the x-ray rocking curve repeatedly (see Fig.13).

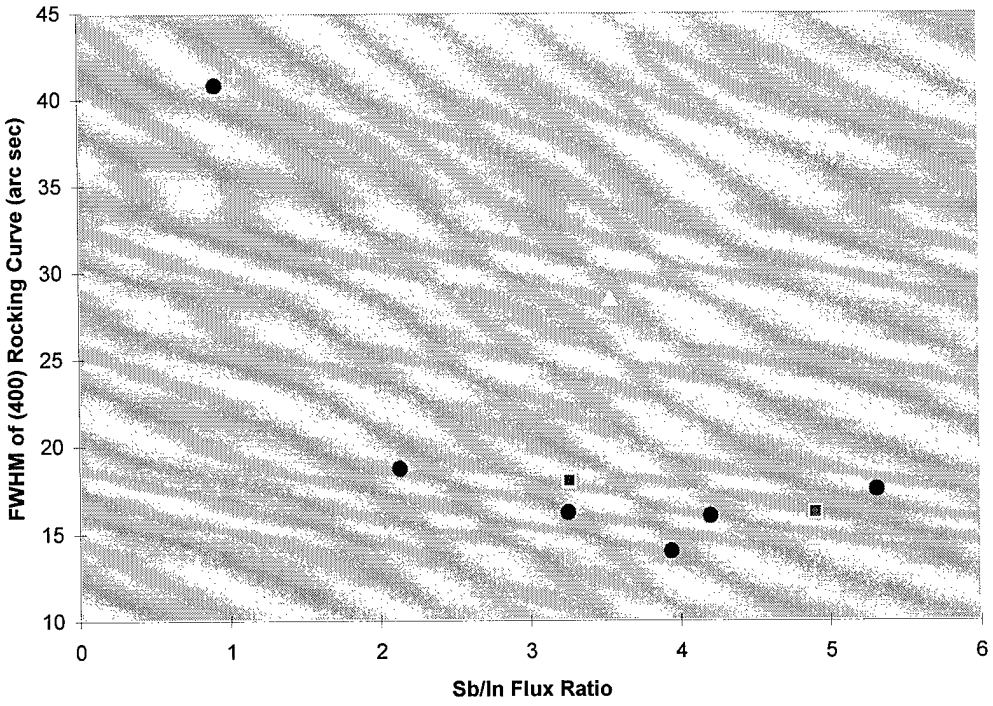

Fig.13. The variation of FWHM from x-ray rocking curve for different Sb/In flux ratios. The points "●" correspond to those grown at 370 °C for different Sb/In BEP ratio. The values of the FWHM do not change significantly with the BEP ratio except when the ratio falls below 2, indicating poor crystalline quality in the In rich condition. The "data points ■" are those grown at 400 °C. The quality of the layers is comparable to the ones grown at 370°C. It may be noted that all the above data were taken on substrates which underwent treatment 4 (Sb flux open after oxide desorption). The data points "▲" refer to the ones grown at temperature 370 °C but on substrates which have been subjected to 2^{nd} and 3^{rd} treatments. X-ray rocking curves for the layers grown on these substrates are wider indicating poor crystalline quality.

Growth kinetics were also studied using RHEED image acquisition and analysis system. The coherent length of growing surfaces were examined at the initial stage of InSb epitaxy as a function of the above different substrate surface treatments. Coherent length is inversely proportional to the width of RHEED diffraction streaks. This width was measured at different time during the initial growth stage. Figure 14 shows these data for different substrate conditions. It was observed that width of the RHEED diffraction streaks increase with the initiation of InSb growth, reaches a peak and appears to saturate at a lower value on surfaces that had undergone treatments 1 and 3. However, for surfaces that used the procedures 2 and 4, the width of the RHEED diffraction monotonically decreased with time after the initiation of the growth. These data suggest the presence of oxide or other crystalline phases causing rougher surface at the beginning of InSb growth, for the surfaces that have undergone treatments 1 and 3 consistent with the earlier x-ray diffraction data.

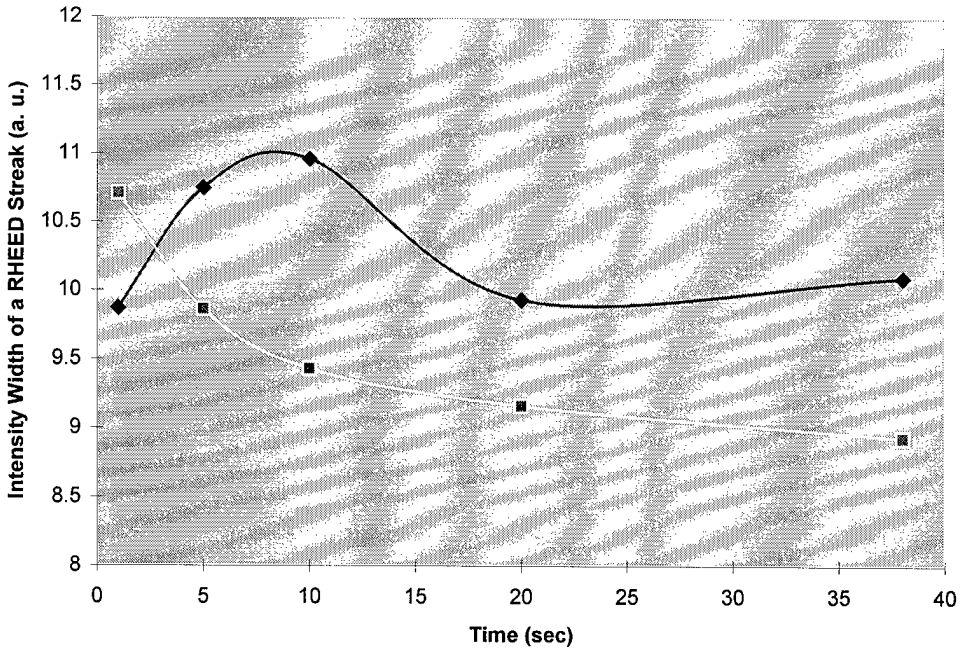

Fig.14. The variation in the intensity width of the RHEED streak with time at the initial growth stage of InSb. "◆" represents the data on subtrates that had undergone treatment 1 and 3, "■" correspond to that of treatment 4.

In conclusion, the thermal desorption process that yields the best InSb surface is different from those observed in GaAs. The introduction of Sb flux, prior to or after the oxide desorption appears to be the critical factor that determines the best surface for the subsequent growth. Thus the surface initially etched in lactic acid:HNO_3:HCl=25:4:1 solution for 90 seconds at room temperature before loading in the system, followed by preheating in the introduction chamber up to 200°C for one hour (to outgas both the Mo blocks and substrates), desorbing the oxide at 440°C in the growth chamber and at 460°C in the presence of Sb flux for 10 minutes, appear to be the best sequence for the homoepitaxial growth of InSb of superior quality.

(c) InSb Homoepitaxial Growth

Study on homoepitaxial growth of InSb has been somewhat limited in the literature as most of the work has been focussed on heteroepitaxial growth of InSb on GaAs [9-11]. No systematic growth investigation has been reported on homoepitaxial growth of InSb. It is interesting to investigate the homoepitaxial growth as the quality of the layers grown on GaAs is dominated by the interface defects due to the large (~14%) lattice mismatch between the two substrates. Hence, the crystalline quality variation caused by changes in growth parameters cannot be properly revealed. On the other hand, the high crystalline quality achieved in the homoepitaxial layers of InSb grown,

particularly in our system, facilitates the observation of any small variations in the structural and optical properties of the layer caused by the changes in the the growth parameters. Hence, we carried out a systematic RHEED study and structural quality of InSb epilayer as a function of group V to III BEP ratio.

The InSb epilayers examined were 2 to 3 μm thick. The thickness were determined using the RHEED oscillation and compared with the results obtained from the cleaved cross-section of the sample under the Nomarski phase contrast microscope and DecTech step height measurement. Figure 15 is the InSb growth rate calibration chart, where it is assumed that In flux is the rate controlling parameter with unity sticking coefficient .

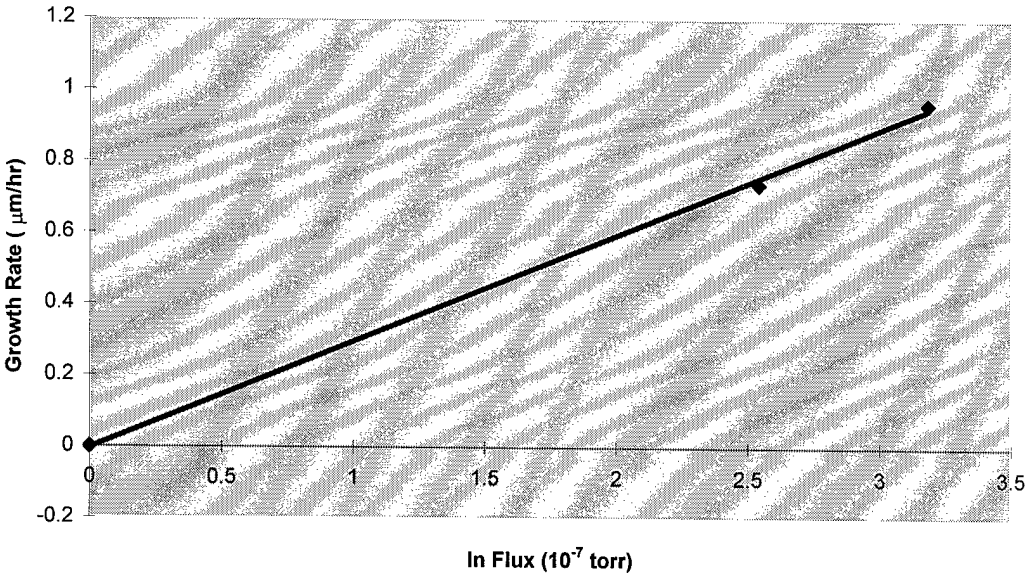

Fig.15. Variation of the InSb growth rate with indium flux.

The epilayers were grown at a substrate temperature of 370°C. For large BEP ratios exceeding 2:1, $(\sqrt{2}x\sqrt{2})45^{\circ}$ surface reconstruction was observed , indicating Sb rich condition. The structural quality of the epilayer was excellent with the FWHM of (400) peak x-ray rocking curve being 14 arc seconds close to the resolution of the x-ray diffraction system. However, surface smoothness was poor. On decreasing the BEP ratio to unity, the surface reconstruction switched from $(\sqrt{2}x\sqrt{2})45^{\circ}$ to pseudo (3x1) RHEED patterns. The surface was mirror smooth though the crystalline quality of the epilayers somewhat deteriorated as indicated in Fig. 13, probably due to the lack of Sb. Epilayers grown at higher substrate of 400°C under Sb rich environment, exhibited comparable quality to those grown at 370°C. But the flux ratio at which the surface reconstruction switched from $(\sqrt{2}x\sqrt{2})45^{\circ}$ to pseudo (3x1) increased, consistent with the earlier reports[6,12]. Thus, the flux ratio appears to have a dominant effect on the surface smoothness and not as much on the structural quality. Unity flux ratio appears to be the lower limit for the growth of epilayers of good structural quality.

The abstract of this work has been submitted for presentation in MRS Fall Meeting, '97. The manuscript for this work is in preparation to be communicated to Appl. Phys. Lett.

D. GROWTH OF GaInAsSb EPILAYERS

GaInAsSb layers were grown on a GaAs substrate with GaSb as a buffer layer. Growth sequence consisted of baking of GaAs substrate in the introduction chamber at 80°C, heating the substrate in the growth chamber at 580°C prior to introduction of any flux to remove any native oxide, and then carrying the growth at 500°C. One half to one μm of GaSb epilayers were grown at this temperature. Growth of GaInAsSb epilayers were initiated at the same substrate temperature by opening simultaneosly the As and In flux shutters. Within three runs of the quaternary growths, epilayers lattice matched to GaSb within 0.2% with an energy gap corresponding to a wavelength of 2.1 μm (as determined from absorption measurements) has been grown. The growth data is tabulated in Table VII.

Table VII. Growth data summary of GaInAsSb epilayers.

Sample Number	#331	#401	#407
V/III. BEP Ratio	6:1	4:1	3.7:1
T_s (°C)	500	500	500
Lattice mismatch(%)	0.4	0.21	-

V. CHARACTERIZATIONS

A. HALL MEASUREMENT

Existing Hall measurement equipment (18+ years old) was restored and upgraded for higher accuracy Van der pauw and Hall measurements, over 10 K to 400 K temperature range and B-field ranges from 10 to 6,000 gauss, to accommodate narrow bandgap III-V materials. The following upgrades were incorporated with some near completion.

- Improved temperature measurement and control by upgrading from single thermocouple to dual silicon group diodes; heater control +/-1.0 K accuracy and sample sensor +/-0.1 K accuracy and by upgrading the temperature controller to a Scientific Instruments 9650 for dual sensors with programmable and IEEE-488 features.
- Improved temperature range and control by upgrading cyrostat coldfinger heater element to higher wattage.
- Improved sample temperature tracking by fabricating improved sample mount with sapphire/indium mounting surface with temperature sensor located adjacent to the DUT.

- Improved low field (E, B) measurement with low E-field control by installing higher sensitivity (microvolt level) Keithley voltmeter and a Keithley 244 precision constant current power supply, respectively and B-field measurement by installing precision Lakeshore Cryotronics 450 gaussmeter.

In addition, lab equipment was acquired and set-up for preparing Hall measurement samples: cleaning, etching, cloverleaf pattern making, annealing and metal dot attachment, wire attachment and mounting.

The equipment performance has been verified, with regards to the accuracy of resistivity and Hall measurements over temperature, for GaSb and InSb MBE grown on GaAs (100) by comparing to those same samples which were and are being evaluated by other labs (University of New Mexico and Wright Patterson Laboratory). The results, as shown in Figs. 16 and 17, have compared well with respect to resistivities and temperature dependent profiles. Similarly, concentration and mobility measurements have also been confirmed. The rapid decrease in resistivity with increase in temperature, starting at about 100 K, has been reported to be due to a dominant parallel conduction channel of low mobility formed by the dislocation region near the InSb/GaAs hetero-interface. The analysis of the low temperature resistivity is nearly impossible without knowing the donor concentration.

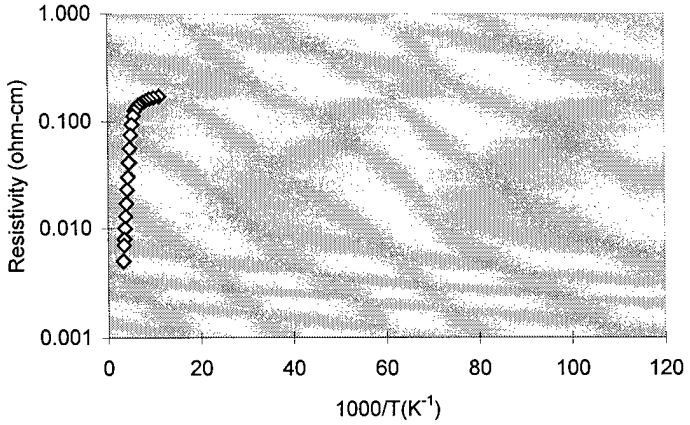

Fig.16. Sample #602 InSb/GaAs (100) resistivity vs. temperature measurements performed at NC A&T SU.

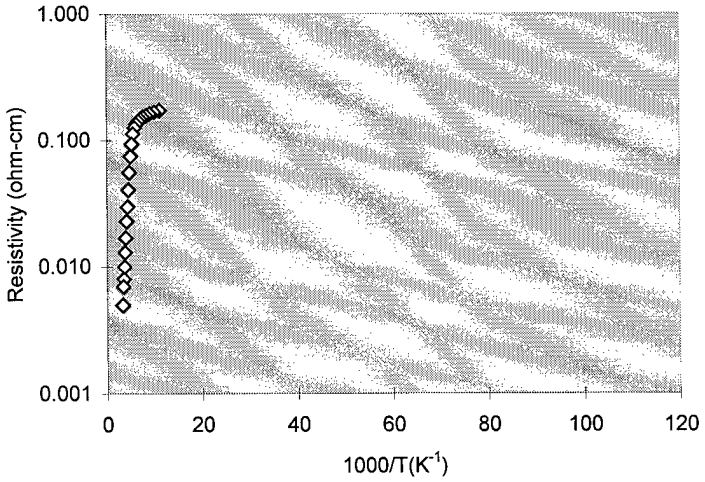

Fig.17. Sample #602 InSb/GaAs (100) resistivity vs. temperature measurements performed at UNM.

B. Low temperature Protoreflectance

Photoreflectance is a very important tool for the evaluation of semiconductor thin films, interfaces, microstructures and actual device structures. The main process is the interaction of electrons with the electric field in the space-charge region. The derivative nature of this technique provides maximum sensitivity to interband electronic transitions and thus to the band structure of the material being investigated.

A standard PR apparatus was already set up in [13] the laboratory from the past funding obtained form AFOSR (Grant # F46920-89-C-004). Using the current funding the system was extended to low temperature. Presently, the sample can be cooled to as low as 4 K by closed cycle Joule-Thompson cryogenic refrigerator system.

We report here the first low temperature PR study of liquid phase electroepitaxially (LPEE) grown GaSb on (100) GaSb substrates in the entire wavelength range, corresponding the energetic values of 1.3 to 1.8 eV, encompassing the spin-orbit-split transition energies ($E_0+\Delta_0$) of the fundamental band gap. The experiment was carried out at low temperatures to obtain sufficient carrier lifetime to effectively modulate the electric field. The samples studied were undoped and Te-doped substrates from two vendors, Metal Specialities and Sumitomo and LPEE grown epilayers. The detailed temperature dependence of these transitions over a temperature range of 4 K to 210 K was also carried out.

No PR signals were obtained on any of the undoped sample in the entire temperature range investigated. Photoreflectance spectrum of a Te-doped GaSb sample corresponding to $E_0+\Delta_0$ transition is shown in Fig.18. The energy peak of the PR signal peak was determined by fitting the experimental curve over a limited energy range to a theoretical low-field approximation[14]

$$\Delta R/R = \mathrm{Re}[Ce^{i\theta}(h\omega - Eg + i\Gamma)^{-n}] \qquad (1)$$

where $h\omega$ is the probe photon energy, and E_g, C, Γ, and θ are the energy, amplitude, broadening parameter and phase, respectively of the structure, while n denotes the type of critical point. The PR spectra was best simulated for n=2 corresponding to the excitonic line shape in all the samples in the entire temperature range investigated. The values are tabulated in Table VIII.

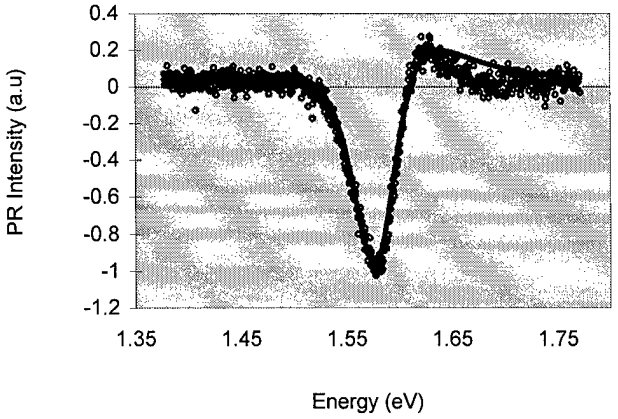

Fig.18 Experimental PR spectra for the $E_0+\Delta_0$ transition in Te- doped GaSb samples supermiposed by theoretically simulated spectra (solid line).

Table VIII. Parameters that yielded best fit to the experimental PR spectra of $E_0+\Delta_0$ transition at 4 K in Te-doped GaSb samples. A first derivative function with excitonic line shape was used for simulation.

Sample	$E_0+\Delta_0$ (eV)	$(\Gamma)_{0+\Delta 0}$ (meV)	FWHM of x-ray rocking curve (arc-sec)
LPEE: Ψ-36	1.611	73	20-24
Ψ-38	1.617	52	29-38
Bulk (sm)	1.603	78	43
Bulk (ms)	1.581	42	18

Vendor: ms= Metal Specialties now known as Epitronics
sm= Sumitomo

LPEE= Liquid phase epitaxially grown epilayer at N.C. A&T State University

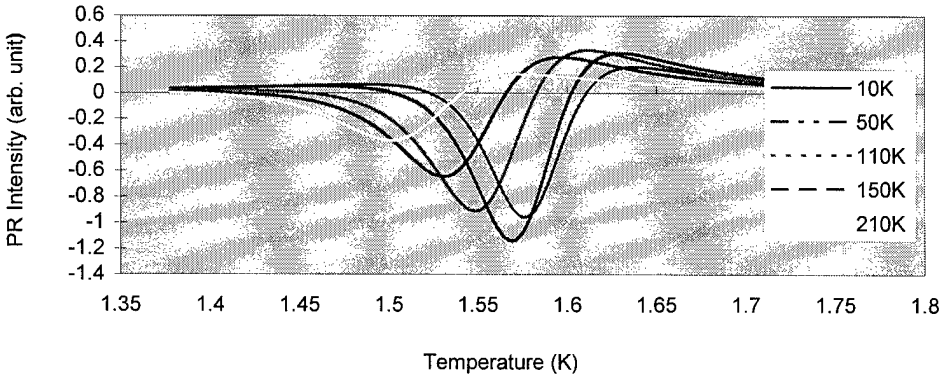

Fig.19. PR spectra of the $E_0+\Delta_0$ transition as a function of temperature

Figure 19 illustrates the temperature dependence of PR spectra for $E_0+\Delta_0$ transition. The intensity of the PR spectra becomes weak as the temperature increases and the PR peak energy shifts towards lower energy with temperature. The shifts of the critical-point energies with temperature are caused by the thermal expansion of the lattice and the renormalization of the band energies by electron-phonon coupling[15].

The temperature induced shifts in the $E_0+\Delta_0$ transitions as illustrated in Fig. 20 in E_0 vs T plot shifts vertically with the sample. We believe that these are similar to the Burstein-Moss shifts due to band filling. The exact values of carrier concentration is not known for these samples, however, the carrier concentrations are in the $(1\text{-}7)\text{x}10^{17}/\text{cm}^3$ range. Semi-empirically derived Varshni's law[16] has been used to describe the temperature dependence of these two critical points.

$$E(T) = E(0)-\alpha T^2/(T+\beta), \qquad (2)$$

where E(0) is the energy of the critical point extrapolated to zero temperature and α and β are empirical fitting parameters. Table IX tabulates the values of E(0), α and β that gave the best fit and are compared with the published data on the fundamental gap. It may be noted that the temperature dependencies are different for both these transitions.

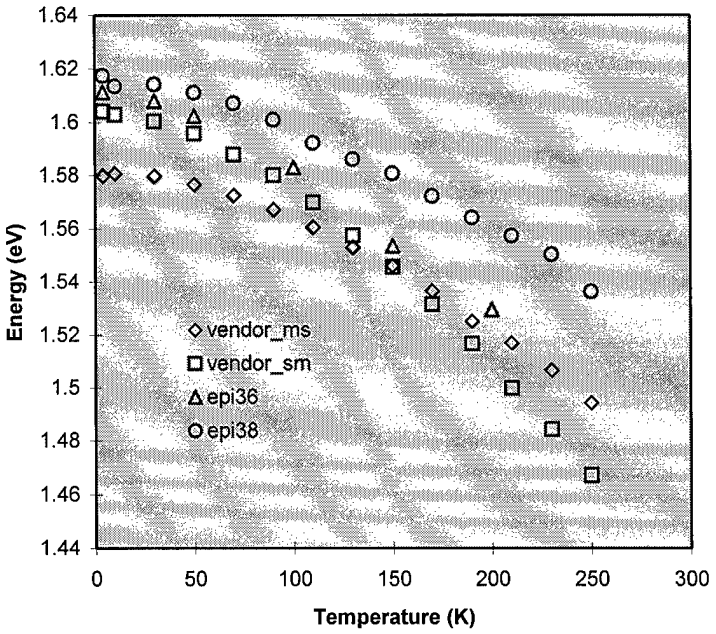

Fig.20. Temperature dependence of PR peak energy

Table IX. Values of the parameters which describe the temperature dependence of the $E_0+\Delta_0$ transitions in Te-doped GaSb

Sample	E(0) (eV)	α (10^{-4} eV/K)	β (K)
Camassel et al.[17]	0.810	3.78	94
Chen et al. [18]	0.812	4.2	140
Te-doped GaSb	1.58-1.60	9-11	~400

Electrolyte electroreflectance (EER) technique was also used to confirm the origin of the PR spectra. The EER spectra for the $E_0+\Delta_0$ transition of a Te-doped GaSb sample is shown in Fig. 21. The results obtained for the Te-doped samples are in essential agreement with previous electrolyte ER[18,19], and Schottky barrier ER[20] data. The energy of the transition determined from fitting Eq. (1) is 1.497 eV.

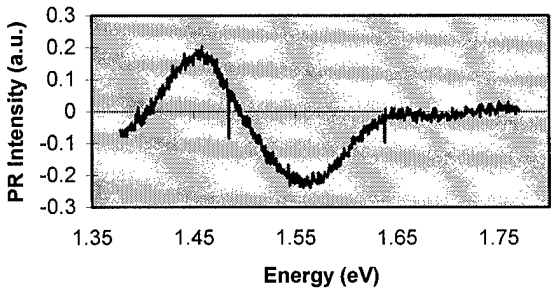

Fig.21 EER spectra for the $E_0+\Delta_0$ transition of a Te-doped GaSb sample

There is a significant difference in the line shapes of the photoreflectance and electrolyte electroreflectance spectra. While usual sharp differential reflectance lines are observed in the EER spectra at room temperature, the PR spectra is broad and do not contain the positive excursion around 1.45 eV. These suggest presence of different mechanisms that give rise to entirely two different signals.

The dependencies of the PR spectra on the incident intensity and the chopper frequency were also examined to determine if any component of thermal reflectance was present in the PR spectra. Intensity of the PR signal varied as cube root of the incident intensity, in excellent agreement with those observed in GaAs samples [21]. No significant changes in the intensity was observed as the chopper frequency was varied. These clearly attest to the fact that the signal is due entirely to the modulation in the built in surface field.

The abstract of this work has been submitted for presentation in MRS Fall meeting. The theoretical interpretation of the entire work is currently under study and will be communicated shortly to J. Appl. Phys.

VI. THEORETICAL INVESTIGATION OF InAsSb/InTlSb SUPERLATTICE

Energy band calculations for a novel superlattice InAsSb/InTlSb lattice matched to InSb has been carried our as it offers a potential application for an infrared detector in the 8-12 μm region. Improvements in the InTlSb epilayers' structural quality are expected as it will be sandwiched between higher quality zincblende InAsSb epilayers. Preliminary energy band calculations of 30Å $InAs_{0.07}Sb_{0.93}$/100Å $In_{0.93}Tl_{0.07}Sb$ SL show the band alignment favorable to type I with three heavy-hole subband confinement in the valence band and a partial electron subband confinement in the conduction band due to the small conduction band offset. Including the effect of strain indicates significant changes in the band offsets, with optical bandgap essentially unaltered. The optical band gap of this SL was computed to be 0.127 eV (9.7 μm) at 0 K, indicating its potential for long wavelength applications.

This work has been published in J. Electronic Materials and the reprint of the paper is attached in Appendix.

This work has been published in J. Electronic Materials and the reprint of the paper is attached in Appendix.

VII. SUMMARY

In summary, epilayers of GaAs, GaSb, InSb and GaInAsSb on GaAs of good quality have been grown using MBE system. Homoepitaxial growth of InSb of excellent structural quality has been grown using a novel oxide desorption procedure. Low temperature PR reflectance on Te-doped GaSb for $E_0+\Delta_0$ transition energy has been obtained. Temperature dependence of this transition is different from the fundamental band gap reported in literature.

Theoretical calculations have been made on InAsSb/InTl Sb superlattice structure. This sturcture has been predicted to exhibit type I band alignment with an energy gap corresponding to long wavelength device applications.

VIII. BIBLIOGRAPHY

1. G. M. Williams, C. R. Whitehouse, C. F. McConville, A. G. Cullis, T. Ashley, S. J. Courtney and C.T. Elliot. App. Phys. Lett. 53(13), 1189(1988).
2. S. E. Hooper, D. I. Westwood, D. A. Woolf, S. S. Heghoyan and R. H. Williams
3. Semicord. Sci. Technol. 8, 1069-1074 (1993) .
4. M.Yano, K. Yamamoto, T. Utatsu and M. Inoue, J. Vac. Sci.Technol.B/2(2),1133(1994)
5. J. F. Klem, J. Y. Tsao, and J. L. Reno, A. Datye and S. Chadda, J. Vac. Sci. Technol. A, Vol.9, No.6, 2996(1991).
6. Philip E. Thompson, John L. Davis, and Ming-Jey Yang, David S. Simons and Peter H. Chi, J. Appl. Phys. 74(11), 6686(1993).
7. Kunishige Oe, Seigo Ando and Koichi Sugiyama, Japanese Journal of Applied Physics, Vol.19, No.7, July, 1980, pp. L417-L420
8. W. K. Liu, and M. B. Santos, J. Vac. Sci. Technol. B, to be published."The Oxide Handbook" (2^{nd} Ed.), Ed. G. V. Samsonov (IFI/Plenum, New York, 1982).
9. P. E. Thompson, J. L. Davis, J. Waterman, R. J. Wagner, D. Gammon, D. K. Gaskill, and R. Stahlbush, J. Appl. Phys. 69(10), 7166(1991).
10. G. M. Williams, C. R. Whitehouse, C. F. McConville, A. G. Cullis, T. Ashley, S. J. Courtney, and C. T. Elliot, Appl. Phys. Lett. 53(13), 1189(1988).
11. C. Besikci, Y. H. Choi, R. Sudharsanan, and M. Razeghi, J. Appl. Phys. 73(10), 5009(1993).
12. A. J. Noreika and M. H. Francombe, C. E. C. Wood, J. Appl. Phys., Vol.52, No.12, 7417(1981).
13. S. Iyer and W. J. Collis, "Optical Characterization of $In_xGa_{1-x}As_ySb_{1-y}$/GaSb Alloy and Device Application", Final Report, Air Force Office of Scientific Research, period Nov. 1, 1988 - Oct. 30, 1992.
14. D. E. Aspnes, Surf. Sci. 37, 418 (1973).
15. S. Gopalan, P. Lautenschlager, and M. Cardona, Phys. Rev. B35, 5577 (1987).
16. Y. P. Varshni, Physica 34, 149 (1967).
17. J. Camassel and D. Auvergne, Phys. Rev. B 12, 3258 (1975).
18. S. C. Chen and Y. K. Su, J. Appl. Phys. 66, (1989).
19. M. Cardona, K. L. Shaklee, and F. H. Pollak, Phys. Rev. 154, (1967).
20. D. E. Aspnes, C. G. Olson and D. W. Lynch, Phys. Rev. B14, 4450, (1976).
21. J. L. Shay, Phys. Rev. B2, 803 (1970).

IX. PUBLICATIONS & THESIS ARISING FROM AFOSR

Refereed Publications

S. Iyer, Jie Li, Shahnaz Chowdhury-Nagle, Yi Zhao, and K.K Bajaj, "InAsSb/InTlSb Superlattice-A Proposed Heterostructure for Long Wavelength Infrared Detectors", J. Electron. Mater. 26,347 (1997).

.S. Iyer, K.K. Bajaj, Shahnaz Chowdhury-Nagle and Jie Li, " Theoretical Study of InTl Sb/InAsSb Superlattice for Far Infared Detector", Presented at the MRS Spring Meeting, San Francisco, (April 8, 1996), Mat. Res. Soc. Symp. Proc. 421, 395(1996).

Non-refereed Publications and Presentations

S. Iyer, J. Li, B. Mangalam, S. Mulugeta, D. Faulk and W. Collis, Low Temperature Photoreflectance of GaSb, MRS Fall Meeting, Boston, MA, Dec.3, 1996.

D. Johri, J.Li and S.Iyer, Calibration of Substrate Temperature and the Source Fluxes in the MBE System, MRS-NC Section Annual Symposium, Microelectronics Center of North Carolina, November 22, 1996

S.Mulugeta, J.Li and S.Iyer, Low Temperature Photorefelectance of GaSb, MRS-NC Section AnnualSymposium, Microelectronics Center of North Carolina, November 22, 1996

S.Venkatraman, J.Li, T. Radownowicz, S.Iyer, A. Rice and S.Hegde, Characterization of (001) GaSb MBE grown epilayers, MRS-NC Section Annual Symposium, Microelectronics Center of North Carolina, November 22, 1996.

S. Iyer, Shahnaz Choudhury- Nagle Jie Li, and K.K. Bajaj " Theoretical Study of InTlSb/InAsSb Superlattice for Far Infrared Detector", APS March Meeting, St. Louis, MO, March l9, 1996.

Shahnaz Choudhury- Nagle, S.Iyer and Jie Li, " Computation of Energy subbands in InTlSb/InAsSb using the modified formalism for the Kronig-Penney models", MRS-NC Section Annual Symposium, Microelectronics Center of North Carolina, November 10, 1995.

Badri Mangalam, Devona Faulk , S.Iyer and Jie Li," Modulation Photoreflectance of Semiconductors" MRS-NC Section Annual Symposium, Microelectronics Center of North Carolina, November 10, 1995.

Other Presentations

S. Iyer, "Antimonide Based Materials", AFOSR Electronic and Optical Materials Review/Workshop, Wright -Patterson AFB, OH, August 23, 1996.

S. Iyer, "Antimonide Growth", FAST IR Sensor Technology Center (FIRST) Program Review, NM, Albuquerque, March 19, 1996.

S. Iyer, "Status of NC A&T SU's New Projects on MBE of Sb Based III-V Alloys: Direction, Needs, Concerns" - Twelfth Baltimore-Washington MBE User's Meeting, NIST, Gaithersburg, MD, Nov. 10, 1993.

Papers Submitted for Presentation

J. Li, S. Iyer and S. Venkatraman , "RHEED Study of Oxide Desorption of InSb" submitted to MRS Fall Meeting, 1997, Boston, MA.

S. Iyer, Solomon Mulugeta, Jie Li, and Badri Mangalam, "Photoreflectance Study of GaSb in the E_0 and $E_0+\Delta_0$ Transition Energies and their Temperature Dependences" submitted to MRS Fall Meeting, 1997, Boston, MA.

Thomas A. Rawdanowicz, Jie Li, S. Iyer, S. Venkatraman and W. J. Collis, "Electrical Properties of MBE Grown InSb and SnTe Doped InSb on GaAs", submitted to TMS 1998 Annual Meeting, San Antonio, TX

Publication in Preparation

1. "RHEED Study of Oxide Desorption of InSb"
2."Photoreflectance study of GaSb in the E_0 and $E_0+\Delta_0$ transition energies and their temperature dependences"
3."Electrical Properties of MBE Grown InSb and SnTe Doped InSb on GaAs"

Graduate Degrees Awarded

TEM, SIMS, SEM and AFM analysis of Te implanted GaSb, Badri Mangalam, 9/95.
Theoretical Study of InAsSb/InTlSb as a Long Wavelength Material, Shahnaz Chowdhury-Nagle, 6/96.
Low Temperature Photoreflectance of GaSb, Devonna Faulk, 7/96
In-Situ MBE Characterization Techniques: RGA and RHEED, Juanita Rhodes, 7/97

Master's Thesis in Progress

Thomas A. Rawdanowicz, " Electrical Properties of MBE Grown InSb and SnTe Doped InSb on GaAs ", to be completed by 9/97.

Solomon Mulugeta, " Photoreflectance Study of Te Doped GaSb in the E_0 and $E_0+\Delta_0$ Transition Energies and their Temperature Dependences" to be completed by 8/97.

X. PARTICIPATING SCIENTIFIC PERSONNEL AND REPORTS SUBMITTED

Faculty

Dr. Shanthi Iyer, Professor
Dr. Ward Collis, Associate Professor
Dr. Jie Li, Research Associate

Graduate Students

Mr. Badri Mangalam, MSEE
Mrs. Shahnaz Chowdhury- Nagle, MSEE
Mrs. Devonna Faulk, MSEE
Ms. Juanita Rhodes, MSEE
Mr. Thomas A. Rawdanowicz, MSEE candidate
Mr. Sreenivasan Venkatraman Ph.D. candidate
Mr. Solomon Mulugeta MSEE candidate

Undergraduate Students
Ms. Nidhi Sangal
Ms. Kim Presley
Ms. Crystal Flemming

Reports Submitted

Annual Report: 1/15/93-7/30/94
Interim Report, Oct.1, 1993 - Sept. 30, 1994.
Annual Report: 1/15/94-1/14/95
Annual Report: 9/1/95-7/31/96

XI. APPENDIX

Journal of Electronic Materials, Vol. 26, No. 4, 1997

InAsSb/InTlSb Superlattice: A Proposed Heterostructure for Long Wavelength Infrared Detectors

S. IYER,* J. LI, and S. CHOWDHURY-NAGLE

Department of Electrical Engineering, North Carolina A&T State University, Greensboro, NC 27411

K.K. BAJAJ

Department of Physics, Emory University, Atlanta, GA 30322

A novel superlattice (SL) heterostructure, comprising of InTlSb well and InAsSb barrier lattice matched to InSb, is proposed for long wavelength 8–12 μm detectors. Improvements in the InTlSb epilayers' structural quality are expected, as it will be sandwiched between higher quality zinc-blende InAsSb epilayers. Preliminary energy band calculations of 30Å $InAs_{0.07}Sb_{0.93}$/100Å $In_{0.93}Tl_{0.07}Sb$ SL show the band alignment favorable to type I with three heavy-hole subband confinement in the valence band and a partial electron subband confinement in the conduction band due to the small conduction band offset. Including the effect of strain indicates significant changes in the band offsets, with optical bandgap essentially unaltered. The optical band gap of this SL was computed to be 0.127 eV (9.7 μm) at 0K, indicating its potential for long wavelength applications.

Key words: InAsSb/InTlSb, long wavelength infrared (LWIR) detector, superlattice

INTRODUCTION

Currently, there is an increasing research interest to find an alternate material in lieu of current industrial standard HgCdTe in the long-wavelength 8–12 μm range, as poor compositional uniformity and thermal instability are some of the well-known problems associated with this material system.[1] Hence, alternatives based on intersubband transition in III-V compounds multilayered structures[2–4] involving GaAs/GaAlAs, GaAs/GaInP, InP/InGaAsP systems and interband transitions based on type II strained layer superlattice (SL)[4,5] with InSb/InAsSb and InAs/InGaSb are being explored. These are in principle more attractive than those composed of II-VI materials, due to the better metallurgical properties, and more mature growth and device processing technologies. However, due to the inherent quantum mechanical limitations and restrictions, these detectors are predicted to remain inferior to those based on HgCdTe infrared detectors.

In recent years, thallium based III-V compounds[6–8] have been proposed as potential candidates for long-wavelength infrared (LWIR) electro-optic receiver and emitter devices. The theoretical work[7,8] on TlP, TlAs, and TlSb suggests that these binaries are lattice matched to InP, InAs, and InSb, respectively, and are the only compounds in III-V systems which are predicted to exhibit negative band gaps. Hence, the corresponding ternary alloys, which should cover a range of band gaps, should encompass the entire long wavelength infrared region. Of these possible ternary alloys, only the growth of InTlSb has been reported in literature.[9–12] However, InTlSb system is predicted to exhibit a large miscibility gap separating the zinc-blende (ZB) compound InSb from the nearly pure TlSb crystal of closed packed structure, thus leaving only a small phase area of stable ZB alloy at low Tl composition. Hence, only dynamic growth techniques such as molecular beam epitaxy (MBE) and metalorganic chemical vapor deposition (MOCVD) can be employed

*(e-mail address: iyer@garfield.ncat.edu)

(Received October 28, 1996; accepted November 27, 1996)

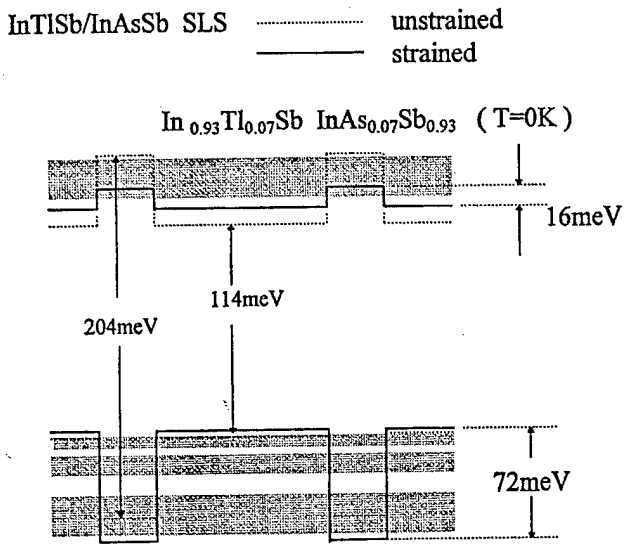

Fig. 1. The bandgap diagram of InAsSb/InTlSb SL with and without the consideration of strain. The effect of strain on the valence and conduction band offsets are opposite, increasing the former and decreasing the latter, respectively.

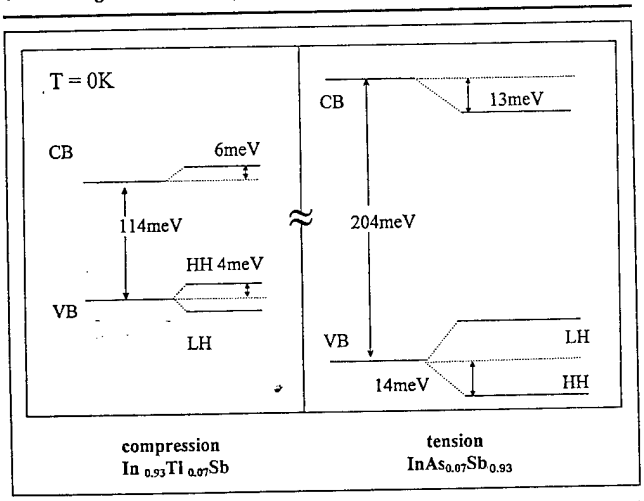

Fig. 2. The effect of strain on the band gap shifts of the InTlSb well and the InAsSb barrier. The heavy-hole band edges shift in the same direction as the conduction band in both the systems, thus leaving the total band offset between the two systems almost unchanged.

for the growth of this alloy system. Preliminary work on the growth of these alloys by MOCVD is quite encouraging,[9,10] and the theoretical calculations of the band structure strongly suggest a marked similarity between HgTe/CdTe and TlSb/InSb systems.

In this paper, we propose a novel $InAs_ySb_{1-y}$/$In_{1-x}Tl_xSb$ SL as a potential candidate for long wavelength detector and emitter applications. Energy band calculations have been made with and without consideration of strain for the heterostructure compositions y = 0.07 and x = 0.07, corresponding to the SL band gap in the wavelength region of 10 μm. Due to the presence of high quality InAsSb layers in this lattice matched SL, it is expected that the structural quality of the system should be superior to that of bulk InTlSb as the latter is reported to be a difficult material to grow.

DISCUSSION

As the material parameters for TlSb is not well established, many of the physical parameters needed for the energy band computation of the heterostructures such as band offsets and effective masses were estimated from the comparison of InTlSb with HgCdTe system. Other ternary material parameters were determined on the basis of linear interpolation from the available binary materials. The linear interpolation method provides a good estimation of the material parameters such as effective mass of compounds in the absence of any empirical data.[13] It is valid for lattice parameter variation with alloy composition (Vegard's Law) and is approximately valid by adding bowing terms in the case of energy band gap parameters variation with composition.

The composition of the InTlSb alloy was thus determined using the above method for an energy gap corresponding to a wavelength of 10 μm. A Tl content of 7% was calculated for a well ($In_{0.93}Tl_{0.07}Sb$) thickness of l_w = 100Å and the barrier ($InAs_{0.07}Sb_{0.93}$) thickness of l_b = 30Å, the mismatch between the free-standing SL and InSb is less than 2×10^{-5}. Thus, we could neglect the strain effect from the substrate on $InAs_{0.07}Sb_{0.93}/In_{0.93}Tl_{0.07}Sb$ SL. The calculated[14] electron and hole effective masses in the InTlSb layer were very close to those of InSb as the Tl content is small. The band offsets in this SL structure were estimated[5,6] from the band offsets of the two individual alloys with respect to InSb independently and thereby calculating the band offsets between the two desired alloy systems assuming the transitivity and commutative properties to hold good. This is a fairly good assumption as it is well proven for this class of materials.[15] The band alignment thus obtained, suggests $InAs_{0.07}Sb_{0.93}/In_{0.93}Tl_{0.07}Sb$ is a type-I SL with a valence band-offset ratio of 62% in a strain-free state, as shown in Fig. 1.

Subband energy calculations were made using modified Kronig-Penney formalism developed by Cho and Prucnal[16] using Bastard's boundary condition. As shown in Fig. 2, these computations in InAsSb/InTlSb superlattice yielded three heavy hole confined subbands. These subbands were located at 4.9, 19.1, and 40.6 meV lower than $In_{0.93}Tl_{0.07}Sb$ valence band maximum, with an increasing band width of 0.09, 4.1, and 11.2 meV, respectively. Note that we merely estimate the heavy hole states in this paper, since they play a more important role than the light hole ones, due to their larger density of states. Only partial electron confinement was obtained in the conduction band with the minimum energy of 7.7 meV above the InTlSb conduction band minimum. The resultant energy gap of the superlattice thus determined was 127 meV corresponding to 9.7 μm in wavelength at 0K.

In order to estimate the strain effects on the SL of 30Å $InAs_{0.07}Sb_{0.93}$/100Å $In_{0.93}Tl_{0.07}Sb$ on InSb substrate, it was assumed that $C_{11} \approx 2C_{12}$ for InTlSb alloy, where C_{11} and C_{12} are the elastic constants and this relation-

ship roughly holds for III-V material system.[13] Contributions due to hydrostatic and shear strain were independently determined. It is assumed that the hydrostatic deformation potentials and shear deformation potentials of InTlSb are about the same as those of InSb due to low Tl content. The hydrostatic part leads to a shift of the average valence-band and conduction-band energies, while the shear contribution in conjunction with the spin-orbit interaction lead to an additional splitting of the valence band energies. As the strain-dependent shift depends on the interface orientation, the calculations were made for (001) substrate. The heavy hole band edge of InTlSb layer shifts toward conduction band under compression, while that of InAsSb layer shifts in the opposite direction, increasing the heavy-hole potential depth and decreasing it for light hole. The strain effect on the conduction band appears more significant because of its small offset (35 meV). As shown in Fig. 2, the overall effect of the strain on the superlattice is to decrease the total conduction band offset, with the valence band offset ratio increased to 80%. However, the superlattice still remains type-I.

The top edges of the heavy hole subbands were computed to be at 6.8, 23.7, and 50.8 meV from the valence band maximum of $In_{0.93}Tl_{0.07}Sb$ with widths of 0.8, 4.3, and 10.5 meV, respectively, with only partial confinement of the subband at 6.5 meV in the conduction band. As shown in Fig. 2, the optical band gap is found to be 126.5 meV, almost the same as that of unstrained SL. In the strained system, the shifts of band offsets in the conduction and valence bands are in the opposite direction, and as a result, the optical bandgap essentially remains unaltered.

As is evident, the strain significantly shifts the band offsets though it does not alter the nature of the SL and the lower subband levels. This leads us to believe that though the estimated band offsets of $InAs_{0.07}Sb_{0.93}/In_{0.93}Tl_{0.07}Sb$ may be approximate due to the lack of available data, the nature of the superlattice will remain type-I and the basic conclusion derived thereof still is a valid one. InTlSb/InSb system is predicted to be similiar to HgCdTe/CdTe system,[17] which also happens to exhibit type-I SL for similar bandgaps. With minor changes in compositions and thicknesses, bandgap of this material system could in principle cover the desired wavelength range of 8–12 μm.

We believe that this structure would allow stability of metastable phase of the InTlSb composition. It has been shown in other systems[18] that metastable phase can be stabilized when sandwiched between high quality zinc-blende structures. The other advantage of this SL structure is that the operating wavelength can be controlled by appropriately changing the thickness of the SL structure. This is much easier to accomplish experimentally in comparison to bulk InTlSb layers of desired composition. Further, the small strain in the SL structure would also assist in the reduction of Auger recombinations, a major limiting factor in the device performance of low band gap materials. Finally, the conduction in this structure could be controlled by doping the InAsSb layer rather than the InTlSb system.

CONCLUSION

In summary, InAsSb/InTlSb SL lattice matched to InSb is predicted to exhibit a type I energy band alignment with the band gap falling into the 8–12 μm wavelength region, and thus is a promising candidate for LWIR detector and emitter materials. Three valence subband confinements and a partial conduction subband confinement have been predicted in 30Å $InAs_{0.07}Sb_{0.93}$/100Å $In_{0.93}Tl_{0.07}Sb$ SL. The strain significantly shifts the conduction and valence band offsets with practically no effect on the operating wavelength.

ACKNOWLEDGMENTS

This work was supported by AFOSR (Grant No. F49620–93–1–0111DEF and F49620–95–1–05).

REFERENCES

1. P.W. Kruse, *Semiconductors and Semimetals* 18, ed. R.K. Willardson and A.C. Beer, (New York: Academic Press, 1981), p. 9.
2. J.M. Kuo, S.S. Pei, S. Hui, S.D. Gunapala and B.F. Levine, *J. Vac. Sci. Technol. B* 10, 995 (1992).
3. S.D. Gunapala and K.M.S.V. Bandara, *Homojunction and Quantum-Well Infrared Detectors* ed. M.H. Francombe and J.L. Vossen, (New York: Academic Press Inc., 1995), p. 113.
4. R.L. Whitney, K.F. Cuff and F.W. Adams, *Semiconductor Quantum Wells and Superlattices for Long-Wavelength Infrared Detectors*, ed. M.O. Manasreh, (Artech House, 1993), p. 55; Christian Mailhiot, ibid, (1993), p. 109.
5. S.R. Kurtz and R.M. Biefeld, *Phys. Rev. B* 44, 1143 (1991).
6. A.B. Chen, M. Van Schilfgaarde and A. Sher, *J. Electron. Mater.* 22, 843 (1993).
7. A. Sher, M. Van Schilfgaarde, S. Krishnamurthy, M.A. Berding and A.B. Chen, *J. Electron. Mater.* 24, 1119 (1995).
8. M. Van Schilfgaarde, A.B. Chen, S. Krishnamurthy and A. Sher, *Appl. Phys. Lett.* 65, 2714 (1994).
9. Y.H. Choi, C. Besikci, R. Sudharsanan and M. Razeghi, *Appl. Phys. Lett.* 63, 361 (1993).
10. P.T. Staveteig, Y.H. Choi, G. Labeyrie, E. Bigan and M. Razeghi, *Appl. Phys. Lett.* 64, 460 (1994).
11. Y.H. Choi, P.T. Staveteig, E. Bigan and M. Razeghi, *J. Appl. Phys.* 75, 3196 (1994).
12. C.E.C. Wood, A. Noreika and M. Francombe, *J.Appl.Phys.* 59, 3610 (1986).
13. M.P.C.M. Krijn, *Semicond. Sci. Technol.* 6, 27 (1991).
14. S. Iyer, S. Chowdhury-Nagle, J. Li and K.K. Bajaj, *Mater. Res. Soc. Symp. Proc.* 421, (Pittsburgh, PA: Mater. Res. Soc., 1996), p. 395.
15. G. Margaritondo, *Electronic Structure of Semiconductor Heterojunctions*, (Kluwer Academic Publishers, 1988), p. 181.
16. H.S. Cho and P.R. Prucnal, *Phys. Rev. B* 36, 3237 (1987).
17. E. Bangert, P. Boege, V. Latussek and G. Landwehr, *Semicond. Sci. Technol.* 8, s99 (1993).
18. Katsuhiro Uesugi, Toshio Obinata, Ikuo Suemune, Hidekazu Kumano and Jun'ichiro Nakahara, *Appl. Phys. Lett.* 68, 844 (1996).

THEORETICAL STUDY OF InAsSb/InTlSb SUPERLATTICE FOR THE FAR INFRARED DETECTOR

S. Iyer*, S. Chowdhury-Nagle*, J. Li*, and K.K. Bajaj**
*Dept. of EE, North Carolina A&T State University, Greensboro, NC 27411, iyer@ncat.edu
**Department of Physics, Emory University, Atlanta, GA 30322, phskkb@physics.emory.edu

ABSTRACT

We propose a novel superlattice (SL) $InAs_ySb_{1-y}/In_xTl_{1-x}Sb$ lattice matched to InSb for a potential application as an infrared detector material in the 8-12 μm wavelength range. We report on the results of energy band calculations for this SL using the modified Kronig-Penney model. Our preliminary calculations indicate that $InAs_{0.07}Sb_{0.93}/In_{0.93}Tl_{0.07}Sb$ would exhibit a type-I SL with conduction band offset of 34 meV and valence band offset of 53 meV at 0K. Due to the lack of accurate information on material parameters, namely, energy offsets and effective masses of InTlSb, these were estimated by comparison with the behavior of HgCdTe system. The theory predicts three heavy hole subbands and one partially confined electron in the 30Å $InAs_{0.07}Sb_{0.93}$/100Å $In_{0.93}Tl_{0.07}Sb$ SL. The band gap of the SL was computed to be 0.127 eV (9.7 μm). It is expected that this SL will allow improvements in the InTlSb epilayers' structural quality as it will be sandwiched between higher quality zincblende InAsSb layers.

INTRODUCTION

There is currently an increasing research interest for a III-V based semiconductor materials as an alternate candidate to HgCdTe for long wavelength (8-12 μm) infrared detectors. One possible series of alloys based on InSb, where the lattice could be dilated by heavier elements such as Bi and Tl, are being considered as potential material systems. Alloying with Bi has posed severe problems in the growth due to the equilibrium alloy miscibility for Bi concentration necessary to achieve narrower band gap [1]. Alloying with Tl is reported [2] to exhibit similar miscibility problem , however the concentration of Tl required to go beyond 10 μm is comparatively smaller. Preliminary work [3,4] on the growth of these alloys by MOCVD are quite encouraging. Hence, of the two, Tl appears to be a more promising element for alloying.

Though the material parameters for TlSb are not well established, the available data and the preliminary calculations of the band structure [5] strongly suggest a marked similarity between HgTe/CdTe and TlSb/InSb systems. Here we propose a new InAsSb/InTlSb superlattice structure on InSb substrate. Many of the physical parameters needed for the computation of hetrostructure such as band offsets and effective masses were estimated from the comparison of the above two alloy systems.

Our preliminary calculations indicate that the proposed structure would exhibit a type I superlattice. The subband structures in $InAs_ySb_{1-y}/In_xTl_{1-x}Sb$ system were calculated by using the modified version of Kronig-Penney model developed by Cho and Prucnal [6] where Bastard's boundary condition was adopted. Calculations have been made for the heterostructure compositions of $y = 0.07$ and $x = 0.93$, which corresponded to the band gap in the wavelength region of 10 μm.

Mat. Res. Soc. Symp. Proc. Vol. 421 © 1996 Materials Research Society

ESTIMATION OF THE PHYSICAL PARAMETERS

In this section a brief review of the similarity between HgCdTe and InTlSb system is presented. The choice of the compositions constituting the superlattice, and the estimation of different parameters required for the energy band calculations of the InAsSb/InTlSb superlattice is described below.

Similarities Between HgCdTe and InTlSb System

Although TlSb has been predicted to slightly favor the CsCl over zincblende structure, alloys of InTlSb towards InSb corner of the phase diagram with Tl content less than 15%, are expected to exhibit a stable zincblende phase with a direct band gap at the Γ point [2,5]. TlSb with zincblende phase is predicted to exhibit a negative band gap. Chen et al. [5] calculated the band gap using local density approximation (LDA) which was found to be in good agreement with the estimated value obtained from tight binding calculations. The inversion to negative gap was found to be -1.5 eV, and the valence band offset in the InSb/TlSb system was predicted to be 20% of the band gap difference, which correlates well with that observed in HgCdTe system. The difference in the band gap between the two end binary compounds in the two alloy systems is also the same ~ 1.8 -1.9 eV. Chen et al. [5] also calculated the energy band structures for HgCdTe and InTlSb alloys at both compositions corresponding to an energy gap of 0.1 eV at zero temperature by using a hybrid psuedopotential tight-binding method. It was found that the two alloys have very similar band structures at this band gap, with similar band gap variation as a function of alloy concentration. Approximately linear shift in band gap with concentration has been predicted for both of these alloys [5]. Thus, all the available evidences suggest strong similarity in the electrical and optical properties of these two systems.

Composition and Thickness of the Epilayers

The composition of the InTlSb alloy was chosen for an energy gap corresponding to a wavelength of 10 μm. This composition corresponded to a Tl content of 7% which was estimated from the linear interpolation of the band gap from TlSb (Eg_{TlSb} = -1.5 eV [2,5]) to InSb (Eg_{InSb} = 0.236 eV).

The thickness of the well ($In_{0.93}Tl_{0.07}Sb$) and the barrier ($InAs_{0.07}Sb_{0.93}$) were calculated so that the entire superlattice is lattice matched to InSb. The thickness of the well and the barrier were thus determined to be 100 Å and 30 Å, respectively.

The Effective Mass

The effective mass variations with band gap are predicted to be similar for both $Hg_{1-x}Cd_xTe$ and $In_xTl_{1-x}Sb$ [5]. The effective mass in HgCdTe decreases with x up to a zero band gap, thereafter increases linearly with composition shift towards CdTe [7]. The zero band gap composition in InTlSb was thus predicted to occur at x = 0.884. We assume that the effective mass of InTlSb alloy interpolate linearly between the end points x = 0.884 and x = 1. Thus the effective mass at the desired composition of x = 0.93 was determined (m^*/m = 0.0139 at 0K). This calculated electron effective mass in InTlSb is very close to that of InSb. Hence, the hole effective mass in InTlSb has been assumed to be the same as that of InSb.

Band Offsets

Finally, the band offsets were determined from estimating the band offsets of the two individual alloys with respect to InSb independently as discussed below and thereby calculating the band offsets between the two desired alloy system.

The valence band maximum of $InAs_{0.13}Sb_{0.87}$ has been reported [8,9] to be 47 meV lower than that of InSb. Assuming that the same fraction of the band gap decrease will be accommodated by the valence band offset in $InAs_{0.07}Sb_{0.93}$/InSb system, the latter is determined to be 29 meV with the valence band maximum of $InAs_{0.07}Sb_{0.93}$ being lower. The valence band offset of InTlSb/InSb is small ~ 20% as per the predictions of Chen et al. [5] and hence the conduction band offset should account for the most of the band gap difference. The valence band maximum of $In_{0.93}Tl_{0.07}Sb$ was thus determined to be 24 meV above that of InSb. As the transitivity property is a common feature and well proven for this class of materials, the valence band offset between $InAs_{0.07}Sb_{0.93}$ and $In_{0.93}Tl_{0.07}Sb$ was estimated to be approximately 53 meV.

Figure 1 illustrates the energy positions of the these two alloys with respect to InSb. As is evident from Fig. 1, InAsSb/InTlSb energy band should be a type I configuration.

Although these are just estimates on the band offsets of $InAs_{0.07}Sb_{0.93}/In_{0.93}Tl_{0.07}Sb$, we believe that the nature of the superlattice will remain unaltered and the basic conclusion derived thereof will remain valid. Further, HgCdTe/CdTe superlattice with similar band gaps is also type I superlattice.

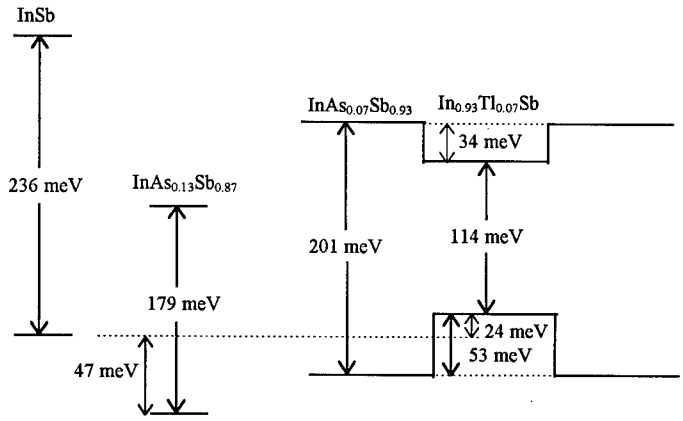

Fig. 1. Energy levels of the conduction and valence bands of the different alloys relative to InSb.

RESULTS

Modified Kronig-Penney formalism [6] with only one boundary condition (Bastard's) at the substrate epilayer interface has been used for the subband energy calculations. This formalism yields envelope wave function corresponding to the minimum and maximum energies of each band. The computations of the band edges by this method are considerably simpler and in the case of GaAlAs/GaAs superlattice, it has been shown [6] to yield results in good agreement with those obtained by conventional Kronig Penny model.

As shown in Fig. 2, calculations on InAsSb/InTlSb superlattice yielded confinement of the first three heavy hole subbands. These subbands were located at 4.9 meV, 19.1 meV and 40.6

meV respectively, deep in the valence band, with a corresponding increasing band width of 0.09 meV, 4.1 meV and 11.2 meV. Only partial electron confinement was obtained in the conduction band with the minimum energy of 7.7 meV. The resultant energy gap of the superlattice thus determined was 127 meV corresponding to 9.7 μm in wavelength.

Due to the presence of high quality InAsSb layers in this lattice matched SL, it is expected that the structural quality of the system should be superior to that of bulk InTlSb, as latter is reported [10] to be a difficult material to grow. Though our focus was on the wavelength close to 10 μm, wavelength over somewhat wider region could be achieved in principle, by varying the layer thickness and the composition of the alloys.

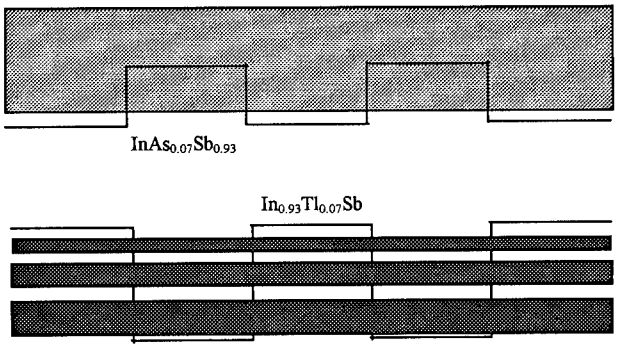

Fig. 2. Conduction and valence subband profiles of the InAsSb/InTlSb type I superlattice.

CONCLUSIONS

In conclusion, InAsSb/InTlSb SL lattice matched to InSb is predicted to exhibit a type I energy band configuration, a desirable result. The SL band gap falls well into the 8-12 μm infrared wavelength region. Three valence subband confinements and a partial conduction subband confinement have been predicted in this SL.

ACKNOWLEDGMENTS

This work was supported by AFOSR (Grant No. F49620-93-1-0111DEF and F49620-95-1-05).

REFERENCES

1. A.J. Noreika, W.J. Takei, M.H. Francombe, and C.E.C. Wood, J. Appl. Phys. 53, 4932 (1982).
2. M.V. Schilfgaarde, A. Sher, and A.B. Chen, Appl. Phys. Lett. 62, 1857 (1993).
3. P.T. Staveteig, Y.H. Choi, G. Labeyrie, E. Bigan, and M. Razeghi, Appl. Phys. Lett. 64, 460 (1994).
4. Y.H. Choi, C. Besikci, R. Sudharsanan, and M. Razeghi, Appl. Phys. Lett. 63, 361 (1993).
5. A.B. Chen, M.V. Schilfgaarde, A. Sher, J. Electron. Mater. 22, 843 (1993).
6. H.S. Cho and P.R. Prucnal, Phys. Rev. B 36, 3237 (1987).

7. P.W. Kruse in Semiconductors and Semimetals, edited by W. Beer, Academic Press, New York, 1981, p. 9-10.
8. S.R. Kurtz, Mater. Res. Soc. Symp. Proc. 216, 163 (1991).
9. S.R. Kurtz and R.M. Biefeld, Phys. Rev. B 44, 1143 (1991).
10. C.E.C. Wood, A. Noreika, and M. Francombe, J. Appl. Phys. 59, 3610 (1986).